

# 1 The *baseless* mutant links protein phosphatase 2A with basal cell 2 identity in the brown alga *Ectocarpus*

3 Olivier Godfroy<sup>1, #</sup>, Min Zheng<sup>2, #</sup>, Haiqin Yao<sup>1</sup>, Agnes Henschen<sup>2</sup>, Akira F. Peters<sup>3</sup>, Delphine  
4 Scornet<sup>1</sup>, Sébastien Colin<sup>2</sup>, Paolo Ronchi<sup>5</sup>, Katharina Hipp<sup>2</sup>, Chikako Nagasato<sup>4</sup>, Taizo  
5 Motomura<sup>4</sup>, J. Mark Cock<sup>1,\*</sup>, Susana M. Coelho<sup>2,\*</sup>

6  
7 <sup>1</sup>Sorbonne Université, UPMC Univ Paris 06, CNRS, UMR 8227, Integrative Biology of Marine Models,  
8 Station Biologique de Roscoff, CS 90074, F-29688, Roscoff, France.

9 <sup>2</sup>Max Planck Institute for Developmental Biology, 72076 Tübingen, Germany

10 <sup>3</sup>Bezhin Rosko, Santec, France.

11 <sup>4</sup>Muroran Marine Station, Field Science Center for Northern Biosphere, Hokkaido University, Muroran,  
12 051-0013, Japan

13 <sup>5</sup>Electron Microscopy Core Facility, European Molecular Biology Laboratory, 69117 Heidelberg,  
14 Germany.

15 <sup>#</sup>joint first authors

16 \*Correspondence: susana.coelho@tuebingen.mpg.de; cock@sb-roscoff.fr

## 17 18 Summary

19 The first mitotic division of the initial cell is a key event in all multicellular organisms and is  
20 usually concomitant with the establishment of major developmental axes and cell fates. The  
21 brown alga *Ectocarpus* has a haploid-diploid life cycle that involves the development of two  
22 multicellular and independent generations, the sporophyte and the gametophyte. Each  
23 generation deploys a distinct developmental program autonomously from an initial cell, whose  
24 first cell division sets up the future body pattern. Here, we show that mutations in the *BASELESS*  
25 (*BAS*) gene result in multiple cellular defects during the first division of the initial cell and  
26 subsequently failure to produce basal structures (rhizoids and prostrate filaments) during both  
27 generations of the life cycle. Cloning-by-sequencing revealed that *BAS* encodes a type B<sup>+</sup>  
28 regulatory subunit of protein phosphatase 2A, and transcriptomic analysis of early  
29 developmental stages uncovered potential effector genes involved in setting up basal cell fate  
30 in this organism. The *bas* mutant phenotype is very similar to that observed in the *distag* (*dis*)  
31 mutants, which lack a functional TBCCd1 protein, at both the cellular and morphological levels.  
32 The high level of similarity of the *dis* and *bas* mutant phenotypes indicate that TBCCd1 and PP2A  
33 are two critical components of the cellular machinery that regulates the division of the initial  
34 cell and mediates the establishment of basal cell fate in the developing thallus.

## 35 Introduction

36 In most animals and plants key events during the first cell division lead to the establishment of  
37 one or more major body axes, providing the foundation for the deployment of the subsequent  
38 steps of multicellular developmental programs (reviewed in (Radoeva et al., 2019; Rose and  
39 Gönczy, 2014). In animals, partitioning defective (PAR) proteins play a key role in establishing  
40 the anterior/posterior body axis, whilst a number of pathways are involved in establishing the  
41 dorsoventral axis (e.g. Mongera et al., 2019). In the land plant *Arabidopsis*, both the apical/basal  
42 axis and apical/basal cell identities are established at the time of the first cell division, and  
43 genetic analysis has identified two main pathways involved in this process (reviewed in Bayer et  
44 al., 2017; Ueda and Berger, 2019). The first pathway involves SHORT SUSPENSOR (an interleukin-  
45 1 receptor-associated kinase/Pelle-like kinase), YODA (a MAP kinase kinase), MPK3 and MPK6  
46 (MAP kinases) and downstream transcription factors, which may include WRKY2 and  
47 GROUNDED/RKD4. This pathway may also be influenced maternally through secreted peptide  
48 factors such as EMBRYO SURROUNDING FACTOR1 and CLV3/ESR-RELATED8. The second  
49 pathway involves auxin and consists of PIN-FORMED 7 (auxin efflux regulator),  
50 MONOPTEROS/AUXIN RESPONSE FACTOR 5 (transcription factor) and BODENLOS/INDOLE-3-  
51 ACETIC-ACID 12 (auxin response inhibitor). The establishment of zygote polarity is a pre-  
52 requisite of the asymmetrical first cell division. This process involves movement of the nucleus  
53 and other organelles, enlargement of the vacuole, and reorganization of microtubules (Kimata  
54 et al., 2016; Ueda and Berger, 2019).

55 The mechanisms underlying the onset of early development from an initial cell in multicellular  
56 plants and animals are relatively well understood, but research has lagged behind for the third  
57 most complex group of multicellular eukaryotes, the brown algae. The brown algae offer an  
58 interesting contrast to animals and plants because of their phylogenetic position and the fact  
59 that they evolved complex multicellularity independently from those groups. Moreover, in  
60 brown algae, the two generations are independent and often very distinct morphologically. The  
61 same genome, therefore, regulates the set-up of two independent and distinct developmental  
62 programs from two different types of initial cells, opening interesting questions about the  
63 molecular control of alternation of generations (Arun et al., 2019; Cock et al., 2014; Coelho et  
64 al., 2007; Coelho et al., 2011). Furthermore, gametophytes and sporophytes of brown algae  
65 develop from single cells outside the parent organism, indicating that they likely establish  
66 polarity in a cell-autonomous manner, without the involvement of factors delivered from the  
67 parental tissues, simplifying the study of polarity, axis establishment and pattern formation.

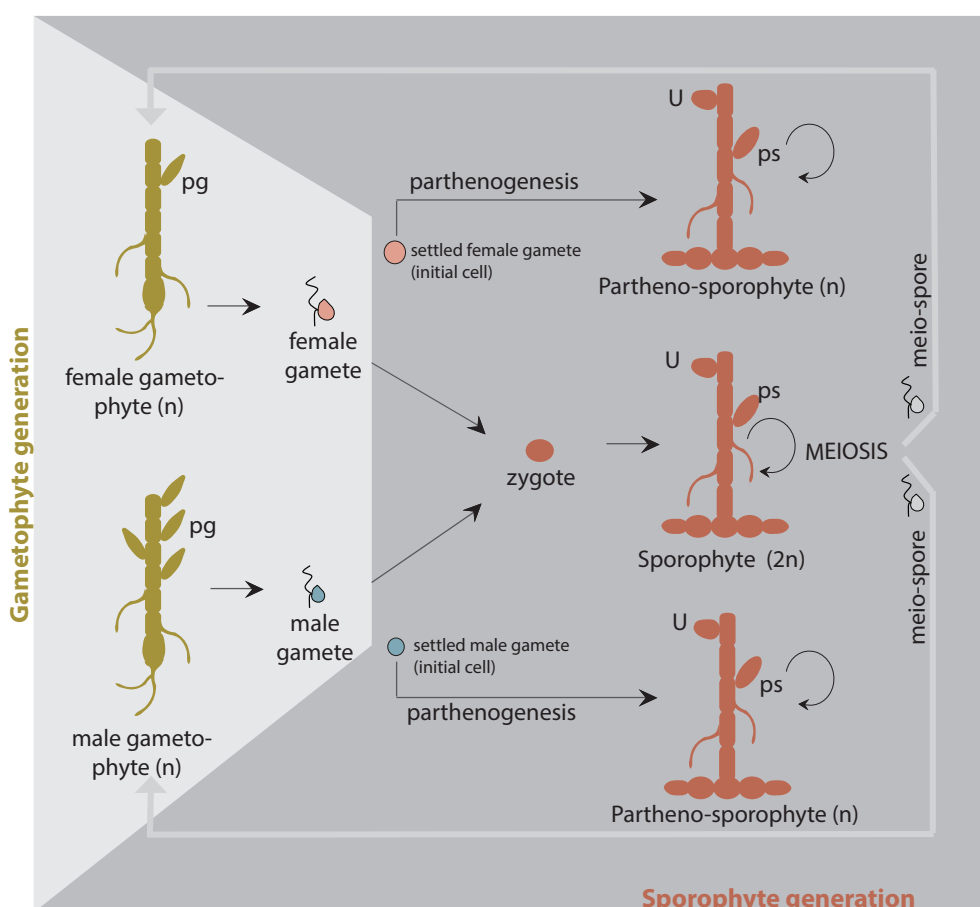
68 Investigations using the brown alga *Fucus* have shown that asymmetrical first cell division is  
69 driven by apical-basal polarity established within the zygotic cell (Brownlee and Bouget, 1998;  
70 Goodner and Quatrano, 1993); reviewed in Bogaert et al., 2022). The two daughter cells of this  
71 first division divide to produce the apical and basal systems of the alga, the thallus and the  
72 rhizoid, respectively (Brownlee and Bouget, 1998). Studies using *Fucus* zygotes have underlined  
73 the role of  $\text{Ca}^{2+}$  asymmetries, mRNA distribution and position-dependent information from the  
74 cell wall (involving an unknown diffusible apoplastic factor) in the determination of the fate of

75 the basal and apical systems (Berger et al., 1994; Bogaert et al., 2022; Bouget et al., 1996;  
76 Brownlee and Bouget, 1998).

77 More recently, *Ectocarpus* has emerged as a suitable model to investigate the molecular  
78 mechanisms underlying initial cell division and cell fate determination in the brown algae  
79 (Bogaert et al., 2022). Advantages of this model include the availability of a range of genetic and  
80 genomic tools (Avia et al., 2017; Badis et al., 2021; Bourdareau et al., 2021; Cock et al., 2017;  
81 Coelho et al., 2020; Cormier et al., 2017; Umen and Coelho, 2019) but also, importantly, the  
82 regularity of the first cell division that characterises the early stages of development of both the  
83 gametophyte and sporophyte generations. In this organism, the gametophyte generation  
84 exhibits an asymmetrical initial cell division that produces a basal rhizoid cell and an apical cell,  
85 the latter further dividing to form the apical system of upright filaments. The upright filaments  
86 bear the reproductive structures (plurilocular gametangia, which produce the gametes by  
87 mitosis). In contrast, the initial cell of the sporophyte generation undergoes a symmetrical initial  
88 cell division to produce two daughter cells with similar fates, both being components of the  
89 basal system (Godfroy et al., 2017; Peters et al., 2008)(Figure 1). The apical system of the  
90 sporophyte (upright filaments) are produced later, after an extensive system of basal filaments  
91 has been established. Reproductive structures (unilocular and plurilocular sporangia) are  
92 produced on the upright filaments.

93 Earlier work identified an *Ectocarpus* mutant, *distag* (*dis*), with abnormal cellular features during  
94 the first cell division, and that was unable to develop basal systems (rhizoids in the  
95 gametophyte, prostrate filaments in the sporophyte)(Godfroy et al., 2017). *dis* mutant alleles  
96 exhibit a strong phenotype in the initial cell, with disordered microtubule networks, larger cell  
97 size, altered Golgi structure and mispositioned nuclei and centrioles (Godfroy et al., 2017). The  
98 cell division plane, however, is normal and the cellular defects are only observed during the  
99 division of the initial cell, suggesting that *DIS* function may be specific to this cell. *DIS* encodes  
100 a Tubulin Binding Cofactor C (TBCC) domain protein of the TBCCd1 class, with conserved roles  
101 in animal and plants (André et al., 2013; Feldman and Marshall, 2009).

102 Here, we report the identification of the *BASELESS* (*BAS*) locus in *Ectocarpus*. *bas* mutants  
103 exhibit phenotypes that closely resemble those of *dis* mutants, including an atypical initial cell  
104 division that leads to failure to deploy a basal system in the adult organism, abnormal cellular  
105 features such as disorganised microtubule cytoskeleton, loss of bipolar germination and more  
106 extensive Golgi apparatus compared with wild-type cells. These phenotypic features are  
107 underlie by important modifications in patterns of gene expression during very early stages of  
108 development. *BAS* encodes a protein phosphatase 2A regulatory subunit type B" with EF-hand  
109 domains. Together, our results are consistent with *BAS* being involved in a pathway that plays a  
110 key role in initial cell division and basal cell fate determination during both the gametophyte  
111 and sporophyte generations of the *Ectocarpus* life cycle.



112

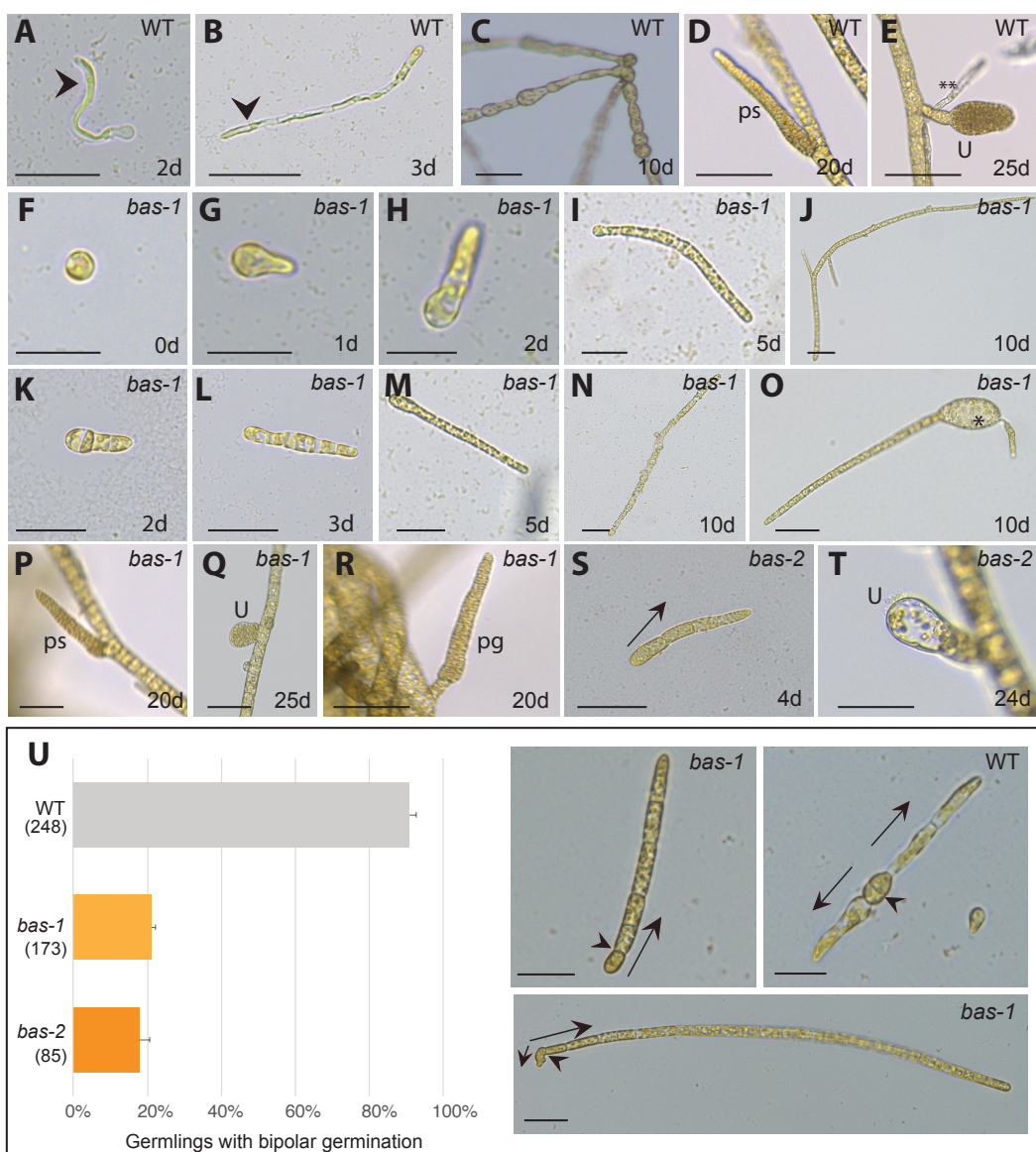
Figure 1. Schematic view of the life cycle of *Ectocarpus* sp.. Like most brown algae, *Ectocarpus* has a haploid-diploid life cycle with haploid, genetic sex determination (Coelho and Cock, 2020; Coelho et al., 2020). Male and female gametophytes produce male and female gametes, respectively, which are released into the seawater from plurilocular gametangia (pg). Gamete fusion produces a zygote which will initiate the (diploid) sporophyte generation. However, gametes that do not meet a gamete of the opposite sex settle and lose their flagella, and they may still function as initial cells of the sporophyte generation because they can develop parthenogenically into a (haploid) partheno-sporophyte. Note that there is no visible (morphological) difference between haploid and diploid sporophytes. Meiosis occurs in the sporophyte (in the unilocular sporangia, U), producing several hundred haploid meio-spores. These meio-spores are released into the seawater and develop into male or female gametophytes. Partheno-sporophytes and diploid sporophytes may also be maintained by production of mito-spores in plurilocular sporangia (ps): released mito-spores recycle the partheno-sporophyte generation (circular arrow in the scheme).

## 113 Results

### 114 **baseless** mutants lack a basal system during both the sporophyte and gametophyte generations

115 During the *Ectocarpus* gametophyte generation, the two cells derived from the division of the  
116 initial cell develop as two germ tubes, and establish a rhizoid (a basal, root-like organ) and an  
117 upright filamentous thallus (an apical, shoot-like organ) (Figure 2A, 2B). The first cell division of  
118 the sporophyte generation, in contrast, produces two daughter cells with similar morphology  
119 and equivalent cell fates (Figure 2C). These two cells then divide to produce a prostrate filament,  
120 which branches to establish the basal system and the apical system differentiates later in

121 development, growing up into the medium from the extensive, prostrate basal system.  
 122 Reproductive structures are produced on the apical system (Figure 2D, 2E).



123

Figure 2. Phenotypes of bas mutants. A) Wild-type gametophyte germling, the arrowhead indicates the rhizoid cell (basal structure). B) Three-day old wild-type gametophyte, the arrowhead indicates the rhizoid. C) Wild-type sporophyte generation composed of round prostrate filaments firmly attached to the substrate. D) Wild-type plurilocular sporangium containing mitotic spores, produced after 20 days in culture. E) Wild-type unilocular sporangium (where meiosis takes place) produced after 25 days in culture. A secondary rhizoid is indicated by asterisks (\*\*). (F-J) Development of the gametophyte generation of the bas-1 mutant. (K-N) Development of the sporophyte generation of bas-1 mutant. O) Occasionally, the mutant strains produced enlarged, abnormal cells (asterisk). P) Plurilocular sporangium on a bas-1 mutant sporophyte. Q) Unilocular sporangium on a bas-1 mutant sporophyte. R) Plurilocular gametangium on a fertile bas-1 gametophyte. S) Initial cell division of a bas-2 gametophyte. T) Aborted unilocular sporangium on a mature bas-2 sporophyte (about 3 weeks after initial cell germination). U) Proportions of 10-day old bas-1 and wild-type germlings that exhibited unipolar germination. Plots represent the mean and SE of five replicate cultures, the total number of germlings scored are indicated in brackets. The photographs are of representative bas-1 and wild-type (WT) germlings, exhibiting uni- (one arrow) or bi-polar (two arrows) germination, respectively. Arrows indicate the direction of germination. Note that, in the bas-1

mutant, following the first cell division, one of the daughter cells continues to divide to produce an upright filament but division of the other daughter cell is arrested. Arrowheads indicate the division plane of the initial cell, which is perpendicular to the growth axis both in the *bas* mutants and in the wild type. *ps*, plurilocular sporangium; *pg*, plurilocular gametangium; *u*, unilocular sporangium. Scale bars=20  $\mu$ m.

124 A screen of a large population of individuals mutagenised by ultraviolet (UV) irradiation  
125 identified two mutant strains (Ec800 and Ec801; Table S1) that failed to develop any of the basal  
126 structures normally observed during either the gametophyte or the sporophyte generation of  
127 wild-type strains (Figure 2). The screen used gametes, which in absence of fertilisation develop  
128 into partheno-sporophytes, being thus initial cells of the sporophyte generation (Figure 1)  
129 (Coelho et al., 2011; Godfroy et al., 2015; Godfroy et al., 2017; Peters et al., 2008). Initial cells  
130 of Ec800 and Ec801 gametophytes immediately developed as apical upright filament cells and  
131 no rhizoid cells were produced. Similarly, during the sporophyte generation, neither mutant  
132 strain produced the network of prostrate basal filaments typical of the wild-type sporophyte  
133 and, instead, the first divisions of the initial cell directly produced an upright filament (Figure  
134 2).

135 In wild-type *Ectocarpus*, secondary rhizoids, which are analogous to the adventitious roots  
136 produced from the stems of some land plants (Atkinson et al., 2014), are produced from apical  
137 upright filament cells at a late stage of development (Figure 2E) (Peters et al., 2008). The Ec800  
138 and Ec801 mutants did not produce secondary rhizoids (Figure 2, Figure S1). Hence, production  
139 of all basal, attachment structures, both primary and secondary, was abolished in these  
140 mutants. Taking into account these phenotypes, the Ec800 and Ec801 mutants were named  
141 *baseless-1* (*bas-1*) and *baseless-2* (*bas-2*) respectively.

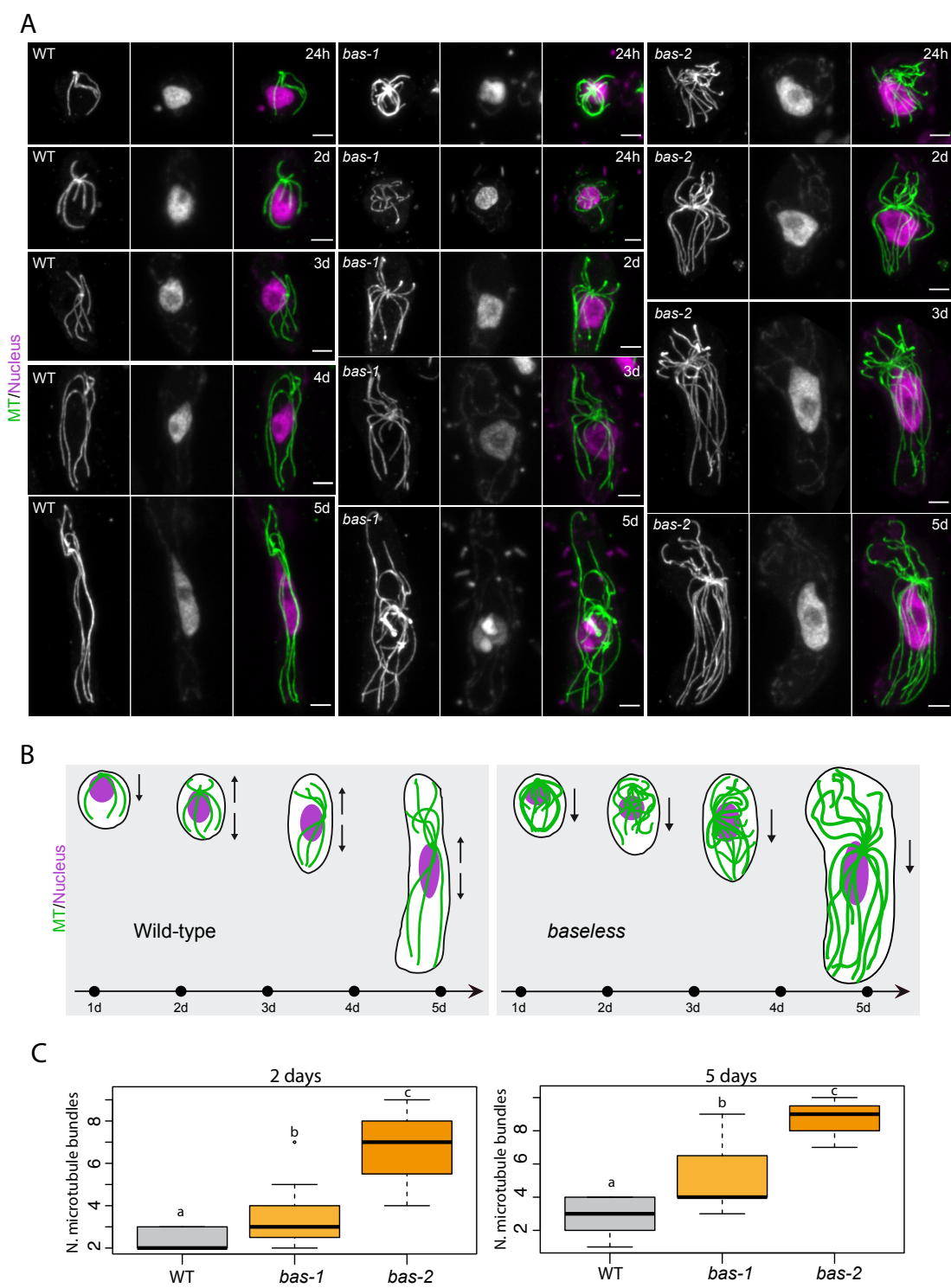
142 The establishment of reproductive structures on apical systems in both the gametophyte and  
143 sporophyte generations was unaffected in the *bas-1* mutant, which was fully fertile after three  
144 weeks in culture (Figure 2F-2S). In the *bas-2* mutant, the formation of the plurilocular sporangia  
145 (which contain mito-spores) was unaffected whereas unilocular sporangia (where meiosis takes  
146 place) aborted and no functional meio-spores were produced, preventing generation of  
147 gametophytes (Figure 2T).

#### 148 ***bas* mutants exhibit reduced bipolar germination compared with wild-type strains**

149 In wild-type *Ectocarpus*, the majority of the initial cells (91%) exhibited a bipolar pattern of  
150 germination, with two germ tubes emerging from opposite poles of the initial cell (Figure 2U;  
151 Peters et al., 2008). In contrast, only 21% of the initial cells of *bas-1* partheno-sporophytes  
152 exhibited this bipolar pattern of germination, the remaining 79% undergoing unipolar  
153 germination (Figure 2U). A proportion of the *bas-1* partheno-sporophytes that exhibited a  
154 bipolar germination pattern produced one or more enlarged and abnormally shaped cells at the  
155 extremity where the second germ tube would normally emerge, possibly corresponding to an  
156 aborted germ tube (Figure 2O). Similar phenotypes were observed for *bas-2* partheno-  
157 sporophytes (Table S2).

#### 158 **Disorganisation of the microtubule cytoskeleton in *bas* mutant initial cells**

159 Mutations at the *DIS* locus strongly affect the organisation of the microtubule cytoskeleton  
160 (Godfroy et al., 2017). Because of the similarity between the morphological phenotypes of *bas*  
161 and *dis* mutants, we investigated the distribution of the microtubule network during early  
162 development of *bas* mutants compared with wild-type germlings (Figure 3A-B). The  
163 microtubule cytoskeleton was markedly disorganised in the *bas* mutants, with supernumerary  
164 microtubule filaments and a disordered network (Figure 3C). This microtubule phenotype is  
165 reminiscent of that of the *dis* mutant (Godfroy et al., 2017). Also, similarly to the *dis* mutant, we  
166 did not detect any abnormalities in the positioning of the cell division plane during early  
167 development; all *bas* initial cells produced a cell division plane perpendicular to the growing  
168 axis (Figure 2U).



169

*Figure 3. The organization of the microtubule cytoskeleton is affected in *bas* mutant germinating cells. A) Confocal maximum z-projections showing representative cells of wild type, *bas-1*, and *bas-2* partheno-sporophytes at several stages of early development (24h, 2-5 days). Microtubules (MT) were immune-stained with an anti-tubulin antibody (green). Nuclear DNA was counterstained with DAPI (mauve). Microtubule (MT) bundles were wavy and more abundant in both *bas-1* and *bas-2* mutant cells compared with the wild-type during the germination of the initial cell. B) Cartoons summarising the stages shown in A) in wild-type and *bas* mutants. C) Number of microtubule bundles during germination in wild-type (WT), *bas-1* and *bas-2* mutants at 2 days and 5 days after germination of the initial cell of the sporophyte generation.*

170 **Ultrastructural analysis of *bas* initial cells**

171 Transmission electron microscopy (TEM) and Focused Ion Beam–Scanning Electron Microscopy (FIB-SEM) were used to further characterise the cellular architecture of *bas* mutants. We 172 focused on the early development of the sporophyte generation, i.e., when unfused gametes 173 had started developing into partheno-sporophytes (2-5 cells), which is the stage when 174 conspicuous morphological differences were observed (Figure 2). This is also the stage when 175 *dis* mutants exhibit altered subcellular phenotypes, including significantly more abundant 176 cisternae and more fragmented Golgi compared with wild-type cells (Godfroy et al., 2017). 177

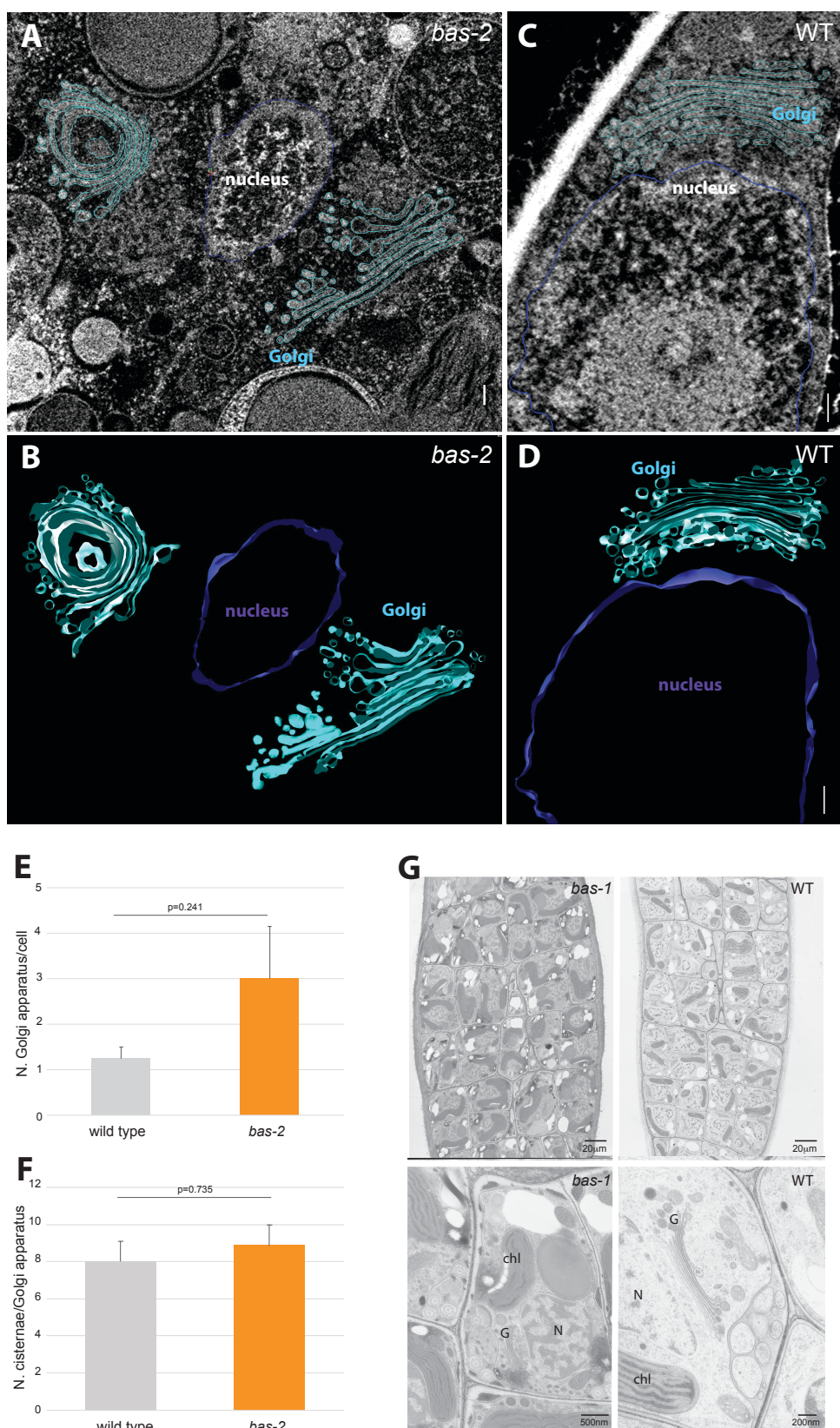
178 Morphometric analyses of the subcellular structures in *bas* mutant and wild-type indicated that 179 the Golgi apparatus were about twice as numerous in *bas* as in wild-type at the same 180 developmental stage, but this difference was not significant (Figure 4E; Table S3). We also 181 noticed that the number of cisternae per Golgi tended to be slightly higher in *bas* (Figure 4F, 182 Table S3). Therefore, *bas* exhibited a Golgi defect, but this defect appeared to be less 183 conspicuous than that of *dis* mutants. We did not observe any other organellar defects in *bas* 184 cells, such as abnormal structure or position of the nucleus, centrioles, mitochondria or 185 chloroplasts. Moreover, no visible defect, in particular at the Golgi, could be observed in the 186 gametes prior to their release from the plurilocular gametangia (Figure 4G). This indicates that 187 *bas* cellular defects are detectable only once the initial cell initiates germination.

188 **Genetic analysis of the *BAS* gene**

189 A male *bas-1* gametophyte (Ec800) was crossed with a wild-type female gametophyte (strain 190 Ec25; (Table S1 and Figure S2). The resulting sporophyte (Ec805) exhibited a wild-type pattern 191 of development, indicating that the *bas-1* mutation was recessive. A segregating family of 38 192 partheno-sporophyte individuals derived from this cross consisted of 16 and 22 phenotypically 193 wild-type and mutant individuals, respectively, consistent with a 1:1 segregation ratio and 194 Mendelian inheritance of a single-locus recessive mutation (Chi-square test with Yates 195 correction = 0.4767, p-value = 0.4899; Table S5). The *bas-1* mutation segregated with the 196 phenotype in the 38 individuals used for the phenotype segregation analysis (Table S4).

197 ***bas-1* and *bas-2* resemble *dis* mutants but are unaffected in the *DIS* gene**

198 The phenotypes of *bas-1* and *bas-2* strongly resembled that of the *dis* mutant (Godfroy et al., 199 2017). The *dis* mutant also fails to produce any basal structures, during both the sporophyte 200 and gametophyte generations, and lacks secondary rhizoids, again during both generations. 201 Sporophytes resulting from crosses either between the *bas-1* strain Ec800 and strains carrying 202 either the *dis-1* or the *dis-2* allele had wild-type phenotypes (Figure S3 and Table S1), indicating 203 complementation, and therefore that the *DIS* gene was not mutated in the *bas-1* mutants.



204

**Figure 4.** Sub-cellular architecture of wild-type and *bas* (*bas-2*) germinating cells. 3D visualization with FIB-SEM (focused ion beam scanning electron microscopy) of representative wild-type (A-B) and *bas-2* mutant (C-D) developing sporophytes (2 cell stage), with Golgi (cyan) and nucleus (violet) highlighted. The scale bar represents 200 nm. E) Number of cisternae per Golgi apparatus in wild-type and *bas-2* developing sporophytes (2 cell stage). F) Number of Golgi apparatus per cell in wild-type and *bas-2* developing sporophytes (2 cell stage). G) Plurilocular

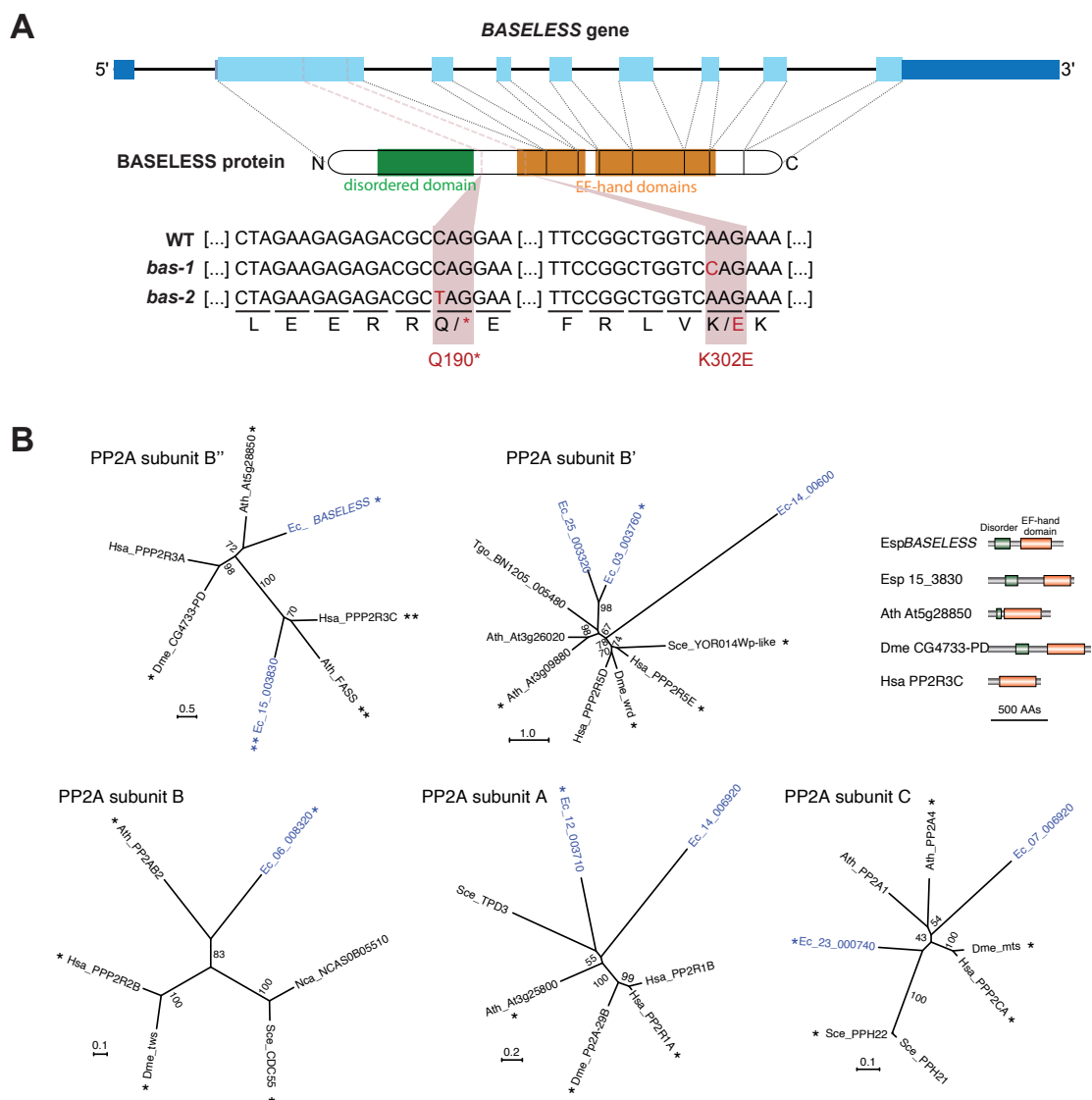
*gametangia in bas-1 and WT, filled with gametes. Note that no difference in the ultrastructure could be observed in the mutant compared with the wild-type samples prior to the release of the gametes from the plurilocular gametangia. Chl: chloroplast, G: Golgi; N: nucleus.*

205 **BAS encodes a protein phosphatase 2A type B" regulatory subunit**

206 Genome resequencing identified a candidate locus on chromosome 21 for the location of the  
207 *bas-1* and *bas-2* mutations (Figure 5). Whole genome resequencing (WGS) was carried out for  
208 the Ec800 (*bas-1*) and Ec801 (*bas-2*) mutant strains and the data compared to the wild-type  
209 *Ectocarpus* sp. strain Ec32 reference genome. More than 41,000 putative variants were  
210 detected for each strain. Those variants were compared to a list of 567,532 variants called  
211 during the analysis of 14 other mutant lines that showed a range of different phenotypes (Table  
212 S5) and shared variants were eliminated. This approach allowed the identification of 827 and  
213 769 variants that were unique to the Ec800 and Ec801 mutants, respectively. Quality filtering of  
214 those variants (see methods for details) resulted in 118 and 67 putative mutations for the Ec800  
215 and Ec801 strains, respectively, corresponding to one mutation every 1.7 to 3.0 Mb of genome.  
216 Of these 185 putative mutations, 26 and 15 were in coding regions (CDS) (22%) in Ec800 and  
217 Ec801, respectively. Only one gene (locusID: Ec-21\_001770) contained a CDS mutation in both  
218 strains. A single nucleotide transition from T to C, at position 2,806,985 was identified in the  
219 *bas-1* mutant (strain Ec800) and a G to A transition at position 2,807,321 in the *bas-2* mutant  
220 (strain Ec801) (Figure 5). The *bas-1* mutation segregated with the phenotype in the 38  
221 individuals used for the phenotype segregation analysis (Table S6).

222 The Ec-21\_001770 gene encodes a protein of 646 amino-acids similar to protein phosphatase  
223 2A regulatory subunit type B" proteins. This polypeptide contains three predicted functional  
224 domains: a disordered region between positions 50 to 185 and two EF-hand domains at  
225 positions 280 to 370 and 380 to 550. The *bas-1* mutation affects the first EF-hand, replacing a  
226 positively charged lysine residue with a negatively charged glutamic acid (K302E). This  
227 modification of electric charge may disrupt domain folding and/or function at least for the first  
228 EF-hand. It is possible that the *bas-1* mutation leads to the production of a protein that is  
229 partially active. The *bas-2* mutant carries a non-sense mutation that creates a premature stop  
230 codon at position 190 of the protein. This mutation is predicted to result in the production of a  
231 truncated protein that lacks both EF-hand domains (Figure 5A).

232 *BAS* is predicted to encode a protein phosphatase 2A regulatory B" subunit. PP2A phosphatases  
233 are protein complexes usually composed of three subunits, a catalytic C subunit, a scaffolding  
234 A subunit and a regulatory B subunit (Wlodarchak and Xing, 2016). Most species have multiple  
235 forms of each subunit and there are four distinct classes of the B subunit (B/B55/PR55,  
236 B'/B56/PR61, B''/PR72/PR130 and B'''/Striatin), which are unrelated at the sequence level. An  
237 analysis of the *Ectocarpus* sp. genome revealed that it encodes B, B' and B" subunits, but not  
238 B'''/Striatin (Figure 5B). The BAS protein is predicted to belong to the B" class, homologous to  
239 the PR130/PR72 human protein (Figure 5B).

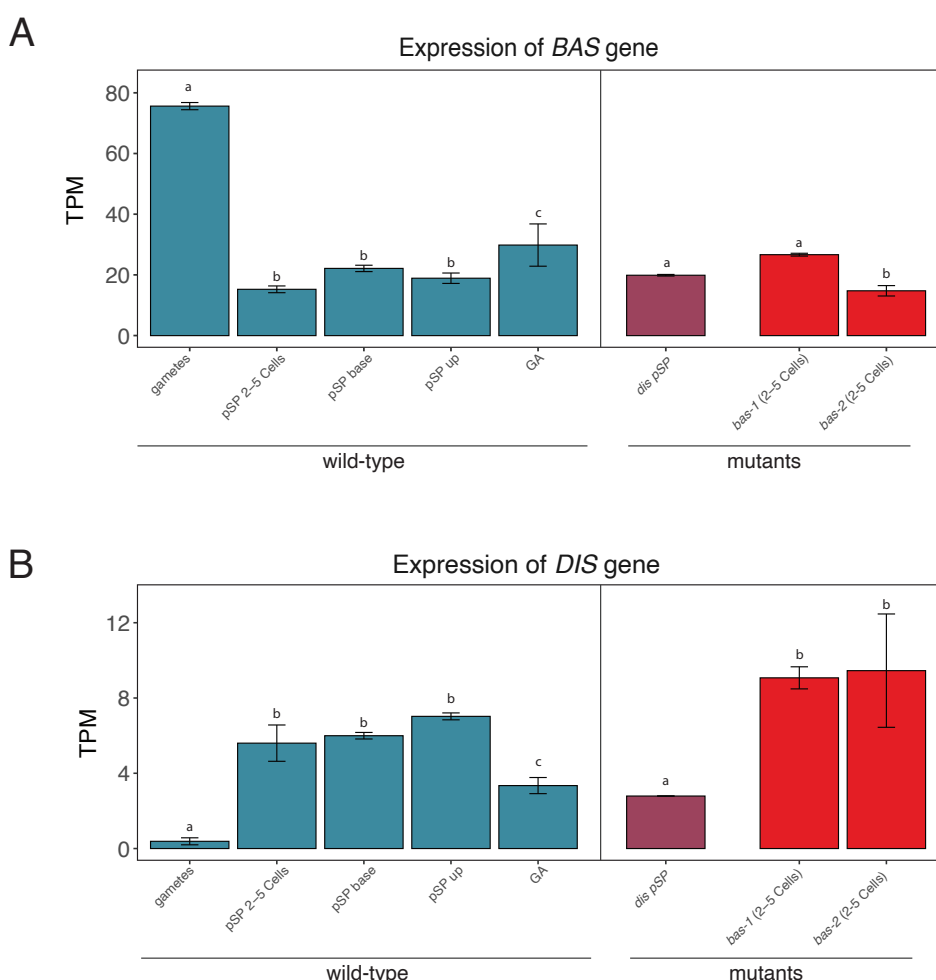


240

*Figure 5. Identification of mutations in the BAS gene and identification of protein phosphate 2A subunits in Ectocarpus. A) Diagram showing the domain structure of the BAS gene, indicating the positions of the bas-1 and bas-2 mutations. The point mutation in exon 2 in bas-1 results in a lysine (K) being replaced with a glutamate (E) residue, whereas the point mutation in bas-2 results in the introduction of a stop codon into the coding region of the gene (represented by an asterisk). Blue boxes indicate exons, with dark-blue representing untranslated regions and light-blue the coding region. B) Ectocarpus protein phosphatase 2A subunits. Unrooted maximum likelihood trees of PP2A subunits (LG+G model). Only bootstrap (1000 repetitions) values of >50 are shown. Ectocarpus proteins are shown in blue. Asterisks and double asterisks indicate best species-to-species reciprocal Blastp matches with the corresponding Ectocarpus protein. The Ectocarpus genome does not encode an orthologue of PP2A subunit B''/striatin. The domain structures of five PP2A subunit B'' proteins are shown with the EF-hand domains in brown and disordered domains in green. AA, amino acid; Esp, Ectocarpus sp.; Tgo, Toxoplasma gondii; Ath, *Arabidopsis thaliana*; Hsa, *Homo sapiens*; Dme, *Drosophila melanogaster*; Sce, *Sccharomyces cerevisiae*; Nca, *Naumovozyma castelli*. Ectocarpus locusIDs are abbreviated as in the following example: Esp\_14\_3830, Ectocarpus sp. Ec-15\_003830.*

241 *BAS expression during Ectocarpus life cycle and in other developmental mutants*

242 RNA-seq data (Bourdareau, 2018; Coelho et al., 2011; Godfroy et al., 2017; Macaisne et al.,  
 243 2017) were analysed to investigate *BAS* gene expression during the *Ectocarpus* life cycle. *BAS*  
 244 transcripts were detected throughout development, during both the gametophyte and  
 245 sporophyte generations (Figure 6A). The *BAS* transcript was most abundant at the gamete stage  
 246 (after the release from plurilocular gametangia) and had decreased in abundance about one  
 247 week after germination, at the 2-5 cell stage (Figure 6A; Tables S7). This pattern of expression  
 248 is consistent with a role of *BAS* in the early divisions of the initial cells of the partheno-  
 249 sporophyte generation provided that the transcript and/or protein persists in the initial cell  
 250 during the first cell division. Interestingly, during the life cycle, the abundance of the *BAS*  
 251 transcript was inversely related to the abundance of the *DIS* transcript, which was at a very low  
 252 level in gametes but increased in abundance at later stages of development (Figure 6, Table S7,  
 253 S8).



254

Figure 6. Abundance of the *BAS* and *DIS* transcripts (measured as transcripts per million, TPM) during the life cycle of *Ectocarpus* and in developmental mutants. A) *BAS* transcript abundance during several developmental stages of wild-type *Ectocarpus* and in *dis* and *bas* mutant strains. Note the high abundance of the *BAS* transcript in gametes. GA: gametophyte, pSP: partheno-sporophyte. Significant differences in expression (Tukey test) are indicated as different letters above the plots, and detailed statistics are presented in Table S14. B) Abundance of the *DIS* transcript in wild-type samples compared with developmental mutants. pSP: partheno-sporophyte; GA:

gametophyte; up, upright filaments of the pSP; base, basal system of the pSP; (2-5 Cells), early development (2-5 cell stage) of the partheno-sporophyte.

255 The similar phenotypes of *dis* and *bas* mutants suggest that the products of the two genes may  
256 play roles in common cellular processes. We investigated the expression of *DIS* in a *bas*  
257 background, and, conversely, the expression of *BAS* in a *dis* background. We noticed that in a  
258 *bas* background, *DIS* expression in early stage (2-5 cell) was significantly higher (p-value=4.13E-  
259 02 and p-value=7.66E-02 respectively for *bas-1* and *bas-2* comparison with wild-type at the 2-  
260 5 cell stage, Figure 6B; Table S7), whereas no difference was observed in the levels of expression  
261 of *BAS* in absence of *dis* gene product. Taken together, these analyses suggest that *BAS*  
262 expression levels are not affected by *DIS*, but, conversely, *DIS* gene expression is disturbed by  
263 mutations at the *BAS* locus. This observation, however, is unlikely to explain the phenotypic  
264 similarity between *bas* and *dis* mutants.

## 265 Analysis of the *bas* transcriptome

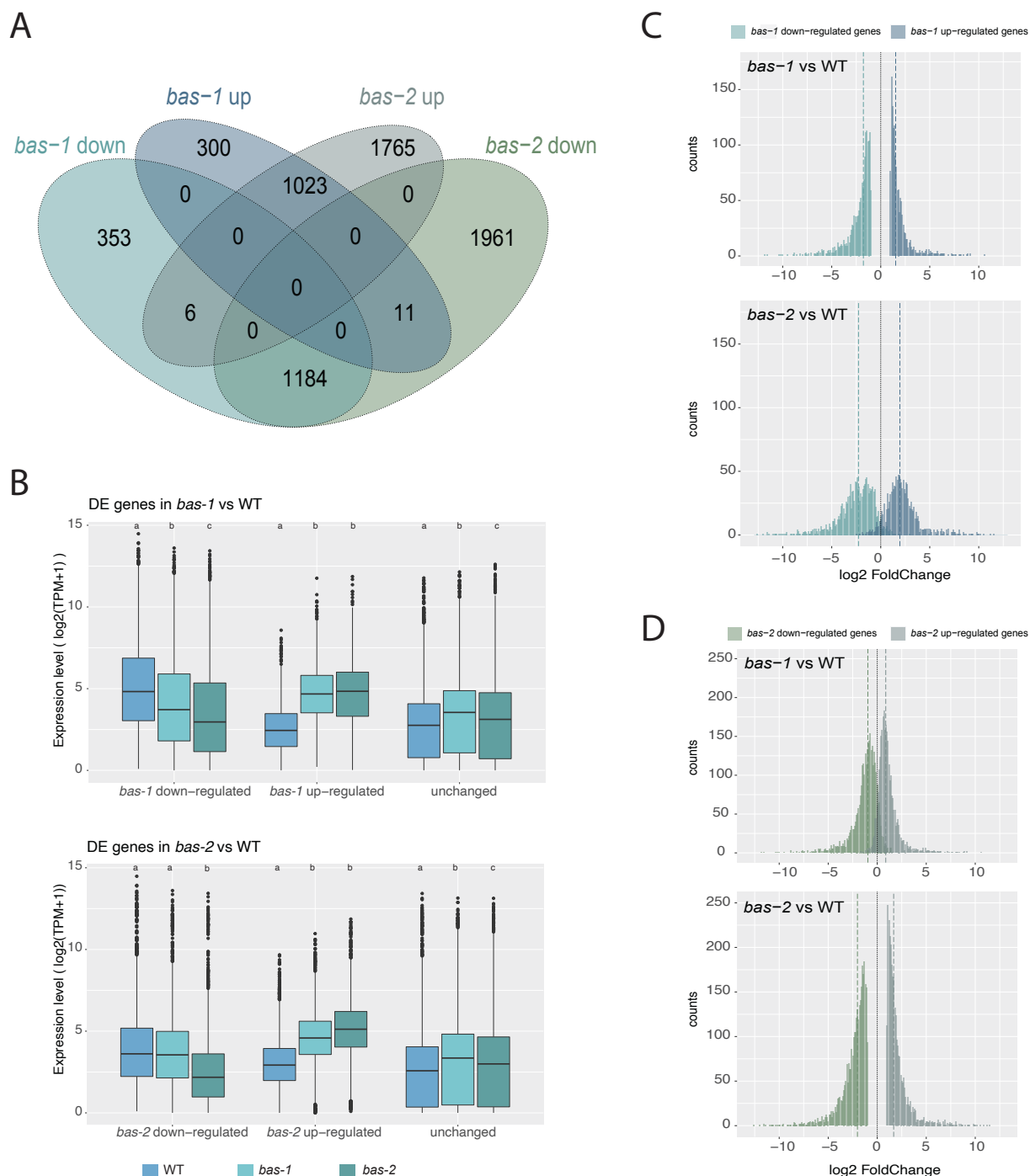
266 To further characterize the *bas* phenotype, an RNA-seq approach was employed to study gene  
267 expression in the *bas-1* and *bas-2* mutants compared with wild-type. We focused on the 2-5  
268 cell stage during gamete germination because the *bas* phenotype was prominent during the  
269 early stages of development. Given the subtle differences in phenotype between *bas-1* and *bas-2*  
270 (in particular the meiotic defect in *bas-2*) we also focused on comparing *bas-1* and *bas-2*  
271 transcriptional patterns.

272 Overall, gene expression patterns in *bas-1* and *bas-2* were comparable, and both were different  
273 from the wild-type samples (Figure S4-S5; Tables S7-S9). However, *bas-2* exhibited more  
274 differences compared with wild-type samples (Figure S4-S5): 40% of the transcriptome was  
275 differentially regulated in the comparison *bas-2* versus wild-type, whereas 20% of the genes  
276 was differentially expressed (DE) between *bas-1* and wild-type (Figure S6, Table S8, see Material  
277 and Methods for thresholds). Most genes were expressed under all conditions, only about 4%  
278 of the genes were not expressed in any of the samples.

279 Differentially expressed (DE) genes exhibited very similar patterns of up and down regulation in  
280 the two *bas* mutants compared to wild-type. Only 11 genes exhibited divergent expression  
281 patterns, i.e., up-regulated in *bas-1* and down-regulated in *bas-2*, and six genes were up-  
282 regulated in *bas-2* and down-regulated in *bas-1*. The vast majority of the DE genes in *bas-1* vs  
283 WT were also differentially expressed in *bas-2* vs wild-type comparison (76.69% of the down-  
284 regulated genes and 76.73% of the up-regulated genes) (Figure 7A, Table S9).

285 Down-regulated genes in *bas-1* compared to wild-type had, globally, lower expression levels in  
286 *bas-2*; and up-regulated genes in *bas-1* were slightly more expressed in *bas-2* (Figure 7B).  
287 Conversely, down-regulated genes in *bas-2* compared to WT had expression levels in *bas-1*  
288 similar to wild-type samples; while up-regulated genes in *bas-2* had intermediate expression  
289 level compare to wild-type and *bas-2* (Figure 7B, Table S9). Comparison of the fold-change  
290 distribution of the DE genes from *bas-1* vs wild-type with those of the DE genes from *bas-2* vs

291 wild-type showed that DE genes exhibited greater fold changes in *bas-2* than in *bas-1* (Figure  
 292 7C, D).



293

Figure 7. Differential gene expression analysis. A) Venn diagram of intersects of DE gene sets in *bas* mutants compare to wild-type. B) Boxplot representation of the distribution of gene expression levels (in  $\log_2$  of TPM values +1) of the DE gene sets from comparisons of either *bas-1* or *bas-2* with wild-type. For each gene category, significant differences in expression level across strains, according to the Wilcoxon test, are indicated as different letters above the plots (details in Table S15). C-D) Histogram representation of the distribution of fold changes of the DE gene sets from comparisons of *bas-1* or *bas-2* with WT; vertical dashed bars indicate the medians of the distributions. DE genes in *bas-1* compared to wild-type (C); DE genes in *bas-2* compared to wild-type (D).

294 Overall, these observations indicate similar changes in transcriptome of both *bas* mutants, with  
295 a stronger effect in *bas-2* than in *bas-1* compared to wild-type. Those results are coherent with  
296 the predicted effects of the two mutations on the *BAS* protein. The *bas-1* mutation may result  
297 in the production of a protein partially active whereas the *bas-2* mutation leads to a truncated  
298 protein with probably no activity.

299 GO term enrichment analyses of DE genes revealed that functions related to photosynthesis  
300 and metabolism were down regulated in both *bas* mutants whereas upregulated genes in  
301 mutants were associated with intracellular protein transport transcription and protein synthesis  
302 (Figure S7, Table S10). It is interesting to note that some of those functions can be linked with  
303 the Golgi apparatus, which appears to be affected by the *bas* mutation (see above). Using the  
304 HECTAR predictor (Gschloessl et al., 2008), we examined the enrichment of DE genes in  
305 particular sub-cellular localizations. In coherence with GO term enrichment analyses, we  
306 observed an enrichment in “chloroplast” localization of the down-regulated genes in both *bas*  
307 mutants. We also observed a slight but strongly significant enrichment in proteins with a “signal  
308 peptide” suggesting an impact of the *bas* mutation on the production of secreted proteins  
309 (Table S11), which, again, may be consistent with defects observed in *bas* mutants at the level  
310 of the Golgi. Finally, we noted that 13 out of the 26 predicted BASIC LEUCINE-ZIPPER (bZIP)  
311 transcription factors in *Ectocarpus* are differentially expressed in *bas-2* mutant compared to  
312 wild-type (Table S9).

313 We identified 26 and 41 genes that were exclusively expressed in the *bas-1* and *bas-2*  
314 respectively compared with the wild-type (i.e., genes that had TMP=0 in wild-type samples).  
315 Seventeen genes were silenced in the *bas-1* and 29 in *bas-2* compared with wild-type (Table  
316 S12 and S13, see Material and Methods for thresholds). Most of those genes have unknown  
317 functions and, due to the low numbers of genes, no significant functional enrichment could be  
318 established. However, it is worth noting several transcription factors, which may be potential  
319 effector genes: such as Ec-14\_003940 and Ec-16\_000350, which are silenced in *bas-1* and/or  
320 *bas-2* and Ec-00\_004890, which is activated in both mutants compared with the wild-type; and  
321 numerous genes associated with “Cellular regulation and signalling” or “Membrane function  
322 and transport”. Looking at the putative localisation of those proteins, we observed that about  
323 30% of the genes specifically silenced in *bas-1* and/or *bas-2* have “signal peptide” or “signal  
324 anchor” prediction, suggested a membrane or cell-wall localization, whereas only 16% of the  
325 total predicted proteins in the genome of *Ectocarpus* present this signature (Table S12). This  
326 two-fold enrichment is even higher than the “signal peptide” enrichment found in down-  
327 regulated genes (Table S11).

## 328 Discussion

### 329 The *BAS* gene is involved in apical-basal axis formation in *Ectocarpus*

330 The two *Ectocarpus* mutant alleles identified in this study, *bas-1* and *bas-2*, lack basal structures  
331 during both the gametophyte and the sporophyte generations of the life cycle. Analysis of the

332 initial cells of the *bas* mutant showed that the morphological phenotype was associated with  
333 several cellular anomalies during germination and the first cell division, including  
334 disorganisation of the microtubule network, an increase in the number of microtubule bundles  
335 and Golgi apparatus and unipolar, rather than bi-polar, germination patterns. These  
336 observations highlight a key role for the BAS protein during the development of *Ectocarpus*. In  
337 particular, the BAS protein appears to operate during key cell divisions during development: the  
338 (first) initial cell division and, at later stages of development, during meiosis. However, no  
339 cellular defect was observed prior to initial cell divisions, suggesting that BAS operates only after  
340 release of the initial cells from the reproductive structures. The meiotic defect observed in the  
341 *bas-2* mutant suggests that the BAS protein may have also a role during meiotic cell division.  
342 The absence of this meiotic defect in the *bas-1* may be explained by the production of a protein  
343 with sufficient activity in *bas-1* to ensure its role during meiosis but not during the first cell  
344 division. Higher penetrance of the *bas-2* mutation is also indicated by the greater proportion of  
345 differentially expressed genes in *bas-2* compared to *bas-1*. Indeed, about 40% of the genome  
346 was significantly mis-regulated in *bas-2* mutant during early stages of development,  
347 demonstrating that mutations at the *BAS* locus can lead to broad, large-scale modifications to  
348 the transcriptome. It is interesting to note that half of the bZIP transcription factors of  
349 *Ectocarpus* are differentially expressed in *bas-2* compared to wild-type. This observation  
350 suggests that BAS may part of a pathway involving additional regulatory proteins that drives the  
351 establishment of apical- basal axis during the early development of *Ectocarpus*.

352 ***BAS* Encodes a PP2A protein with roles in cellular organization and development in animals and**  
353 **plants**

354 *Ectocarpus BAS* is predicted to encode a PP2A phosphatase regulatory B" subunit. In animals,  
355 PP2A phosphatases are involved in diverse cellular processes and constitute a major component  
356 of cellular serine/threonine phosphatase activity, dephosphorylating several hundred cellular  
357 substrates (Reynhout and Janssens, 2019; Wlodarchak and Xing, 2016). PP2A has been  
358 implicated in the reorganization of several cellular structures, playing key roles in nuclear  
359 envelope breakdown during mitosis, and chromosome segregation via effects on assembly of  
360 the mitotic spindle and attachment of cytoplasmic microtubules to kinetochores. It is also  
361 involved in rearrangement of endoplasmic reticulum and the Golgi apparatus (reviewed in  
362 (Wlodarchak and Xing, 2016; Wurzenberger and Gerlich, 2011). In particular, the PP2A B"  
363 subunit PR130 associates with CG-NAP that localizes to centrosomes and the Golgi apparatus  
364 (Takahashi et al., 1999), and restacking of newly formed Golgi cisternae requires  
365 dephosphorylation of Golgi stacking proteins by PP2A (Tang et al., 2008). More broadly, the  
366 animal PP2A B" subunit is critical for cell-cell communication, cell adhesion, migration,  
367 proliferation and differentiation during animal development (Creyghton et al., 2005;  
368 Zwaenepoel et al., 2010). Altogether, these observations link animal PP2A to roles in cell  
369 division, subcellular features and developmental pattern formation. In the multicellular brown  
370 alga *Ectocarpus*, our results are consistent with a similar role for PP2A in subcellular  
371 organisation, cell division and cell fate determination. Our results therefore provide an example

372 of protein functional conservation across eukaryotes that evolved multicellularity  
373 independently, suggesting that the role of PP2A in multicellular development has likely been  
374 preserved across very divergent lineages.

375 Consistent with a conserved role for PP2A in development across multicellular eukaryotes, the  
376 *Arabidopsis* B''- $\delta/\epsilon$  subunit of PP2A (At5g28900/At5g28850) interacts with BASIC LEUCINE-  
377 ZIPPER (bZIP) transcription factors, and is implicated in leaf and root development as well as  
378 mechanical stress response (Tsugama et al., 2019; Van Leene et al., 2016). The PP2A regulatory  
379 B'' subunit FASS/TON2, is essential for the reorganisation of cortical microtubular arrays into a  
380 dense preprophase band preceding cell division. FASS-containing PP2A complexes are targeted  
381 to microtubules through an association with TONNEAU1 (TON1) and TON1-recruiting motif  
382 protein (TRM) (Spinner et al., 2010). PP2A interacts with and dephosphorylates KATANIN, a  
383 evolutionarily conserved microtubule-severing enzyme, to promote the formation of  
384 circumferential cortical microtubule arrays in *Arabidopsis* (Ren et al., 2022). The *Ectocarpus* BAS  
385 protein is related to the *Arabidopsis* FASS/TON2 protein but is orthologous to the AtB''- $\delta/\epsilon$   
386 protein mentioned above (At5g28900/At5g28850). The microtubule phenotype we describe  
387 here, where PP2A B'' disruption in brown algae is associated with microtubule disorganisation,  
388 may further underline a conserved role for PP2A across plants and brown algae.

389 Golgi vesicle transport has been shown to play an important role in the establishment of the  
390 *Fucus* zygote polar axis prior to the first cell division (reviewed in Bogaert et al., 2022; Shaw and  
391 Quatrano, 1996)). It has been proposed that the selective targeting of Golgi vesicles to the  
392 plasma membrane locally modifies the cell wall, participating in the establishment of the  
393 asymmetry of the cell wall required for rhizoid differentiation (Bogaert et al., 2013; Bogaert et  
394 al., 2022; Goodner and Quatrano, 1993). In this model, the cell wall plays a key role in the  
395 establishment of the initial cell asymmetry, which is interesting with regard to the dramatic  
396 changes in expression of numerous genes with putative “Membrane and transport” functions  
397 in *bas* mutants.

398 In animals, the B'' class of PP2A B subunit is thought to be involved in  $\text{Ca}^{2+}$  signalling through  
399 the presence of multiple EF-hand domains (Xu et al., 2010). Note that two EF-hand domains are  
400 predicted in the BAS protein, and these EF-hands are absent or non-functional in *bas* mutants,  
401 suggesting that  $\text{Ca}^{2+}$  binding may be disturbed. In the brown alga *Fucus*,  $\text{Ca}^{2+}$  gradients have  
402 been shown to have a crucial function in zygote polarization and the establishment of the  
403 apical/basal axis during first cell division (reviewed in (Bogaert et al., 2022; Brownlee and  
404 Bouget, 1998). In particular, cytosolic free  $\text{Ca}^{2+}$  accumulates on the side of the growing (basal)  
405 rhizoid, directly linking intracellular  $\text{Ca}^{2+}$  signaling and acquisition of basal cell identity. In this  
406 context, we can speculate that the BAS protein may be a potential sensor of a pre-germination  
407  $\text{Ca}^{2+}$  signal.

408 **BAS and DIS may act in concert to mediate cell fate determination during the first cell division**

409 Similar morphological and cellular phenotypes were observed for *bas* and *dis* mutant strains  
410 suggesting that *BAS* and *DIS* may be involved in similar cellular processes. However, some

411 differences between the mutants are also apparent, such as the less marked Golgi  
412 fragmentation and no effect on nuclear positioning in early stages of development in *bas*, and  
413 also a meiotic defect was only observed in *bas-2*.

414 *DIS* is predicted to encode a TBCCd1 protein. This protein shares similarity with TBCC, which is  
415 a component of the complex (TBCA to TBCE) that mediates dimerization of  $\alpha$  and  $\beta$  tubulin  
416 subunits to form microtubules (Nithianantham et al., 2015; Tian et al., 1996). However, TBCCd1  
417 lacks a conserved arginine residue that is essential for TBCC activity and is unable to  
418 complement TBCC in yeast indicating that the two proteins may have different biochemical  
419 functions (Goncalves et al., 2010). TBCCd1 has been localized to both the centrosome and the  
420 Golgi in humans, *Chlamydomonas*, and trypanosomes and there is evidence that TBCCd1 plays  
421 important roles in positioning organelles within the cells of these diverse organisms (André et  
422 al., 2013; Feldman and Marshall, 2009; Goncalves et al., 2010). However, the molecular  
423 mechanisms underlying these cellular phenotypes are unclear and they may not involve direct  
424 effects on microtubule assembly (Goncalves et al., 2010).

425 Interestingly, analysis of human protein phosphatase interactions revealed that TBCCd1 is a  
426 partner of PP2A regulatory subunit B" (Huttl et al., 2015; Huttl et al., 2017; Yadav et al.,  
427 2017). If this interaction also occurs in brown algae, it would provide a mechanism whereby *DIS*  
428 and *BAS* could act within the same pathway involved in cell fate determination, with *BAS*  
429 regulating the *DIS* protein. Further analysis of the biochemical functions of *BAS* and *DIS* will be  
430 necessary to test this hypothesis.

431 To summarise, both TBCCd1 and PP2A have been linked to cytoskeleton and Golgi function and  
432 both proteins have been shown to play important roles in the regulation of cellular architecture  
433 in diverse eukaryotic systems. These observations are consistent with the pleiotropic cellular  
434 phenotypes of both the *dis* and *bas* mutants. We suggest that the observed morphological and  
435 cell fate (loss of basal cells) phenotypes of the *bas* and *dis* mutants are a consequence of cellular  
436 defects during the first cell division, perhaps through disruption of the distribution of  
437 hypothetical cell-fate-determining factors during this critical step of development (see model  
438 proposed by (Godfroy et al., 2017). Combining information about the *Ectocarpus* *DIS* and *BAS*  
439 proteins with observations of  $\text{Ca}^{2+}$  waves in the *Fucus* embryo, we can speculate that *BAS* may  
440 be involved in sensing an intracellular  $\text{Ca}^{2+}$  signal which participates to the distribution of a cell-  
441 fate determining factor through reorganization of cytoskeleton and Golgi function involving *DIS*.

## 442 Methods

### 443 UV Mutagenesis and isolation of mutant strains

444 Strain cultivation, genetic crosses, raising of sporophytes from zygotes, and isolation of meiotic  
445 families were performed as described previously (Coelho et al., 2012a; Coelho et al., 2012b;  
446 Coelho et al., 2020; Godfroy et al., 2017). *Ectocarpus* sp. (species 7, Montecinos et al., 2017)  
447 gametes are able to develop parthenogenically to produce haploid partheno-sporophytes,  
448 which are identical morphologically to the sporophytes that develop from diploid zygotes

449 (Bogaert et al., 2022; Bothwell et al., 2010; Peters et al., 2008). This phenomenon was exploited  
450 to screen directly, in a haploid population, for mutants affected in early sporophyte  
451 development. UV mutagenesis of gametes was performed as described previously (Coelho et  
452 al., 2011; Godfroy et al., 2015; Godfroy et al., 2017) and mutant partheno-sporophytes lacking  
453 basal structures were identified by visual screening under a light microscope. Table S1 describes  
454 the strains used in this study.

455 **Genetic analysis of *bas* mutants**

456 Genetic crosses were performed as in (Coelho et al., 2012a). The *bas-1* mutant (Ec800) was  
457 crossed with the outcrossing line Ec568 to generate a segregating population of 38 individuals.  
458 Each of the 38 individuals was derived from a different unilocular sporangium (each unilocular  
459 sporangium contains 50–100 meio-spores, derived from a single meiosis followed by at least  
460 five mitotic divisions). The meio-spores germinated to produce gametophytes, which were  
461 isolated and allowed to produce gametes which germinated parthenogenically. The resulting  
462 partheno-sporophytes were then observed under a light microscope to determine whether  
463 they exhibited the *bas* phenotype. The presence of the *bas-1* mutation was determined by  
464 Sanger sequencing of PCR products (Forward: TGACGAATGATGCTAACTGGA, Reverse:  
465 GACAACGGAGCAGACGAAC) for each of the 38 individuals. The *bas-2* mutant (Ec801) was not  
466 usable for crosses because it did not form functional unilocular sporangia, which are required  
467 for gametophyte production.

468 **Identification of candidate mutations**

469 Genomic DNA from Ec800 and Ec801 strains was sequenced on an Illumina HiSeq4000 platform  
470 (1/12<sup>th</sup> lane; 2x150nt paired-end; 8.50 and 7.95 Gbp of data, respectively; Fasteris, Switzerland).  
471 After quality cleaning using Trimmomatic (Bolger et al., 2014), the reads were mapped onto the  
472 *Ectocarpus* sp. reference genome (Cormier et al., 2017) using Bowtie2 (Langmead and Salzberg,  
473 2012). Coverage depth and breadth were, respectively, 34x and 96.83% for Ec800 and 32x and  
474 96.81% for Ec801. Variants were called and counted using bcftools mpileup  
475 (<http://samtools.github.io/>). These variants were compared with a list of variants identified in  
476 genome sequence data for 14 other *Ectocarpus* mutant lines in order to remove false positive  
477 mutations due, for example, to errors in the reference genome sequence.

478 Variants unique to strains Ec800 and Ec801 were quality filtered based on coverage depth ( $\pm 50\%$   
479 of the genome mean), mapping quality ( $>20$ ), variant quality ( $>50$ ), variant frequency ( $>0.9$ ) and  
480 variant support in both sequencing directions. A custom python script allowed the identification  
481 of variants in coding regions (CDS) and the effect of each CDS mutation on the predicted protein  
482 was accessed manually (Table S5). A scheme of the approach is depicted in Figure S7.

483 **Immunostaining**

484 *Ectocarpus* samples were processed as described (Coelho et al., 2012c) using a protocol  
485 adapted from (Bisgrove and Kropf, 1998). Briefly, *Ectocarpus* cells were settled on cover slips  
486 and at appropriate times after settlement were rapidly frozen in liquid nitrogen and fixed in  
487 2.5% glutaraldehyde and 3.2% paraformaldehyde for 1 h, then washed in PBS and treated with

488 5% triton overnight. Samples were then rinsed in PBS and 100 mM NaBH<sub>4</sub> was added for 4 h.  
489 Cell walls were degraded with cellulase (1% w/v) and hemicellulase (4% w/v) for 1 h, and the  
490 preparation was then rinsed with PBS and blocked overnight in 2.5% non-fat dry milk in PBS.  
491 Samples were treated with an anti-tubulin antibody (1/200th, DM1A; Sigma-Aldrich) at 20°C  
492 overnight and then treated with the secondary antibody (AlexaFluor 488-conjugated goat anti-  
493 mouse IgG; Sigma-Aldrich; 1:1000 in PBS) at 20°C overnight. The preparation was rinsed with  
494 PBS and blocked overnight in 2.5% non-fat dry milk in PBS and then treated with an anti-centrin  
495 antibody (1/1000th anticentrin 1 ab11257; Abcam) at 20°C overnight, followed by the  
496 secondary antibody (1/1000th AlexaFluor 555-conjugated goat anti-rabbit IgG; Sigma-Aldrich)  
497 for 8 h. Samples were stained with 4',6-diamidino-2-phenylindole (DAPI; 0.5 µg/mL in PBS) for  
498 10 min at room temperature and mounted in ProLong Gold (Invitrogen).

499 **Confocal Microscopy**

500 Confocal microscopy was conducted using an inverted SP8 laser scanning confocal microscope  
501 (Leica Microsystems) equipped with a compact supply unit which integrates a LIChroic scan  
502 head, several laser lines (405 and 488 nm), and standard photomultiplier tube detectors. We  
503 used the oil immersion lens HC PL APO 63×/1.40 OIL CS2. The scanning speed was set at 400 Hz  
504 unidirectional. The pinhole was adjusted to one Airy unit for all channels. The spatial sampling  
505 rate was optimized according to Niquist criteria, generating a 0.058 × 0.058 × 0.299-µm voxel  
506 size (xyz). The Z-stack height fitted the specimen thickness. A two-step sequential acquisition  
507 was designed to collect the signal from three or four channels. The first step recorded the anti-  
508 tubulin fluorescence signal (excitation, 488 nm; emission, 530 nm) and the transmitted light.  
509 The second step acquired the DAPI fluorescence signal (excitation, 405 nm; emission, 415–480  
510 nm). Signal intensity was averaged three times. The Fiji software was used to optimize the raw  
511 images, including maximum intensity projection and de-noising (3\*3 median filter). For any  
512 given data, both wild-type and mutant images were analysed simultaneously with similar  
513 settings.

514 Tracking of microtubule bundles was performed on maximum intensity projections of z-planes  
515 covering the whole thickness of the cells. We drew a line transversely, perpendicular to the  
516 growth axis of the cell and crossing the nucleus. Peaks corresponding to the microtubule  
517 bundles were then identified in plots of intensity profiles and counted, in order to estimate the  
518 number of microtubule bundles in each cell. Note that in the *bas* mutants, due to the  
519 disorganized nature of the microtubule network, average bundle numbers may be somewhat  
520 underestimated. This is because this method is well adapted for tracking microtubule bundles  
521 oriented with their long axis parallel to the image plane, but we may have missed bundles that  
522 were perpendicular to the plane of the transection.

523 **TEM and FIB-SEM**

524 For transmission electron microscopy (TEM) and focused ion beam-scanning electron  
525 microscopy (FIB-SEM), freshly released gametes were collected in cellulose capillaries and  
526 cultivated in the capillaries in Provasoli-enriched seawater for 3 to 5 days at 14°C in the dark or

527 approximately 1 day at 14°C in 12 h light/12 h dark regime to produce two- to five-cell stage  
528 partheno-sporophytes. Cells in capillaries were frozen at high-pressure (HPF Compact 03,  
529 Engineering Office M. Wohlwend GmbH), freeze-substituted (AFS2, Leica Microsystems) with  
530 0.2% OsO<sub>4</sub> and 0.1% uranyl acetate in acetone containing 5% H<sub>2</sub>O as substitution medium  
531 (Read et al., 2021) and embedded in Epon. Ultrathin sections were stained with uranyl acetate  
532 and lead citrate and analysed with a Tecnai Spirit (Thermo Fisher Scientific) operated at 120 kV.  
533 In order to identify a region of the sample containing algae at high density for FIB-SEM data  
534 acquisition, a 3D X-ray tomogram of the resin block was acquired with a Bruker Skyscan 1272.  
535 The region of interest was exposed using a 90°diamond trimming knife (Cryotrim 90, Diatome)  
536 mounted on a Leica UC7 ultramicrotome. The sample was then attached on a stub using  
537 conductive silver epoxy resin (Ted Pella) and gold sputter coated (Quorum Q150RS).  
538 FIB-SEM imaging was performed with a Zeiss Crossbeam 540 or a Crossbeam 550, using Atlas  
539 3D (FIBICS, Carl Zeiss Microscopy) for sample preparation and acquisition. After the deposition  
540 of a protecting platinum coat on the surface above the region of interest, a 60 µm wide trench  
541 was opened to identify and image several cells in parallel. During the stack acquisition, FIB  
542 slicing was done with at 30 kV and 700 pA current. The datasets were acquired at 8 nm isotropic  
543 voxel size with the SEM at 1.5 kV and 700 pA current, using a back-scattered electron detector  
544 (ESB). After acquisition, the image stacks were acquired using the Fiji plugin “Linear stack  
545 alignment with SIFT” (Lowe, 2004). We acquired images for a total of 5 cells for wild-type and 5  
546 *bas-2* cells, and chose a representative image to present in Figure 4. Images containing Golgi  
547 stacks were retrieved from aligned image stacks and cropped to reduce the image dimensions  
548 for further segmentation with the IMOD software package (<https://bio3d.colorado.edu/imod/>).

#### 549 **Phylogenetic trees**

550 Multiple alignments were generated with Muscle in MEGA7 (Kumar et al., 2016). Phylogenetic  
551 trees were then generated with RAxML (Stamatakis, 2014) using 1000 bootstrap replicates and  
552 the most appropriate model.

#### 553 ***BAS* and *DIS* gene expression estimation during the *Ectocarpus* life cycle**

554 Expression levels of the *BAS* and *DIS* genes were investigated using TPM values obtained after  
555 kallisto pseudo-mapping and calculation of the lengthScaledTPM using the tximport package in  
556 R (see ‘Comparative Transcriptome Analyses’ section for details). Previously generated RNA-seq  
557 data for wild type and *dis* samples (Table S7) was used for comparisons.

#### 558 **Comparative transcriptome analyses**

559 RNA-seq analysis was performed to compare the abundances of gene transcripts in the mutants  
560 *bas-1* and *bas-2* and wild-type sporophytes. RNA-seq datasets were generated from triplicate  
561 samples of each genotype, and individuals were grown synchronously as described previously  
562 in standard culture conditions (Coelho et al., 2012b; Cossard et al., 2022). Germlings were  
563 filtered through a nylon mesh to recover only thalli at the 2-5 cell stage. Each replicate contained  
564 between 10<sup>4</sup> and 10<sup>6</sup> individual germlings. Tissue samples were rapidly frozen in liquid nitrogen

565 and processed for RNA extraction. Total RNA was extracted from each sample using the Qiagen  
566 Mini kit as previously described (Lipinska et al., 2015). For each replicate, cDNA was produced  
567 by oligo(dT) priming, fragmented, and prepared for stranded 2× 150-bp paired-end sequencing  
568 on an Illumina HiSeq 3000 platform.

569 Raw and cleaned read quality was evaluated using fastQC (v. 0.11.9) and mutliQC (v. 1.9). Raw  
570 reads were trimmed and filtered based on quality score, and adapter sequences were removed  
571 using Trimmomatic (v. 0.39). Transcript abundance was evaluate using kallisto (v. 0.46.2) via  
572 pseudo mapping on CDS features. Then matrix of counts and TPMs for all samples, all replicates  
573 were generated in R using tximport package.

574 A gene was considered to be expressed if the TPMmean was above the 5<sup>th</sup> percentile (as in  
575 Cossard et al., 2022; Lipinska et al., 2019). About 4% of the genes in each sample had TPMmean  
576 values under this threshold and were considered not to be expressed in our samples (Table S9).  
577 Differential gene expression was analysed using DESeq2 (Love et al., 2014, 2). Genes were  
578 considered to be differentially expressed when the log2 fold change was below or equal-1  
579 (down-regulated, at least twice as weakly expressed) or above or equal to 1 (up-regulated, at  
580 least twice as strongly expressed) and adjusted p-value below or equal to 0.01. Genes were  
581 considered to be exclusively (uniquely) expressed in *bas* mutants when they were significantly  
582 up-regulated compared to wild-type and the wild-type mean TPM was equal to 0. Conversely,  
583 genes were considered to be specifically silenced in *bas* mutants when there were significantly  
584 down-regulated compared to wild-type and their TPM means were equal to 0.

585 GO term and HECTAR localisation enrichment were carried out on R using the “clusterProfiler”  
586 package (Yu et al., 2012).

## 587 Accession Numbers

588 Accession numbers are provided in Table S7.

## 589 Acknowledgements

590 This work was supported by the CNRS, Sorbonne Université, the Max Planck Society and the  
591 European Research Council (grant agreement 864038 to SMC). HY was supported by a grant  
592 from the China Scholarship Council (grant number 201608310119). We thank Nana Kinoshita-  
593 Terauchi (Shimoda Marine Research Center, University of Tsukuba) and Iris Kock (MPI Tübingen)  
594 for helpful discussion and images of the mutants and Viktoria Buhnets for help with  
595 segmentation of Fib-Sem images.

## 596 Author contribution

597 S.M.C, J.M.C and O.G conceived the project. O.G., M.Z. and S.M.C. performed the main  
598 experimental work. O.G. performed bioinformatic analyses. J.M.C. carried out gene annotation  
599 and phylogenetic analyses. Y.H., M.Z, A.H, A.F.P performed experiments. S.C. and D.S. generated  
600 epifluorescence images. P.R. and K.H. generated and analysed Fib-Sem data. C.N and T.M

601 generated TEM images. O.G., J.M.C. and S.M.C. interpreted the data. S.M.C. wrote the  
602 manuscript with input from all authors.

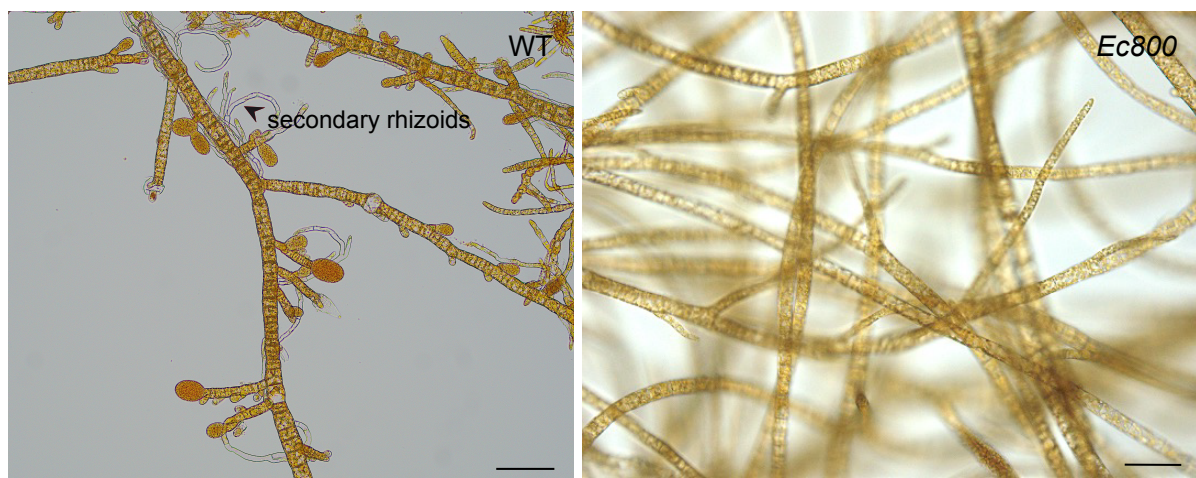
603

604 **Supplemental Figures**

605

606

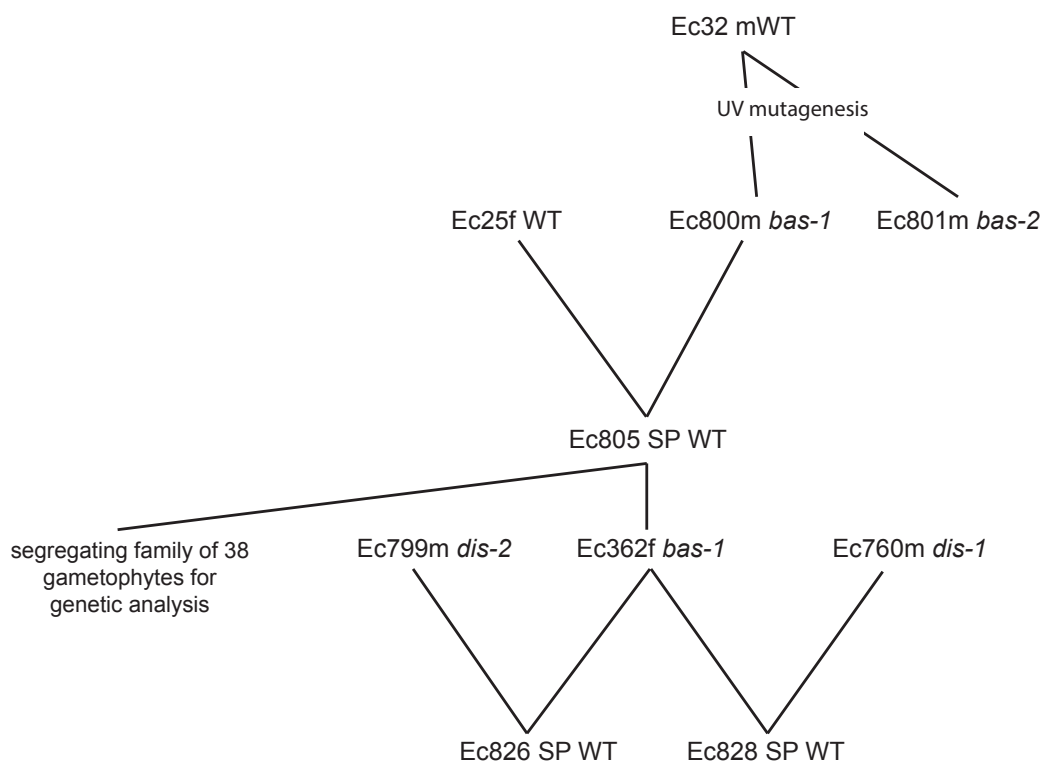
607 **Figure S1.** Absence of secondary rhizoids in apical filaments of mutant lines compared with wild-  
608 type, after 3-weeks in culture. Scale=20  $\mu$ m.



609

610

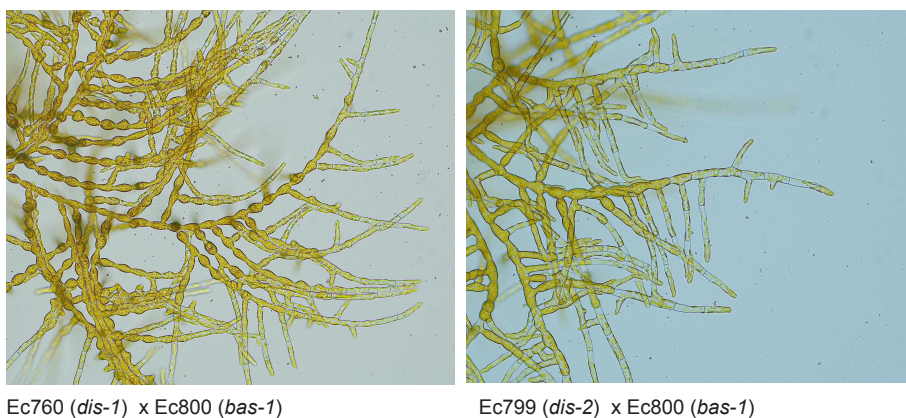
611 **Figure S2.** Pedigree of the *Ectocarpus* strains used in this study. SP, diploid, hybrid sporophyte;  
612 WT, wild type; m, male; f, female.



613

614

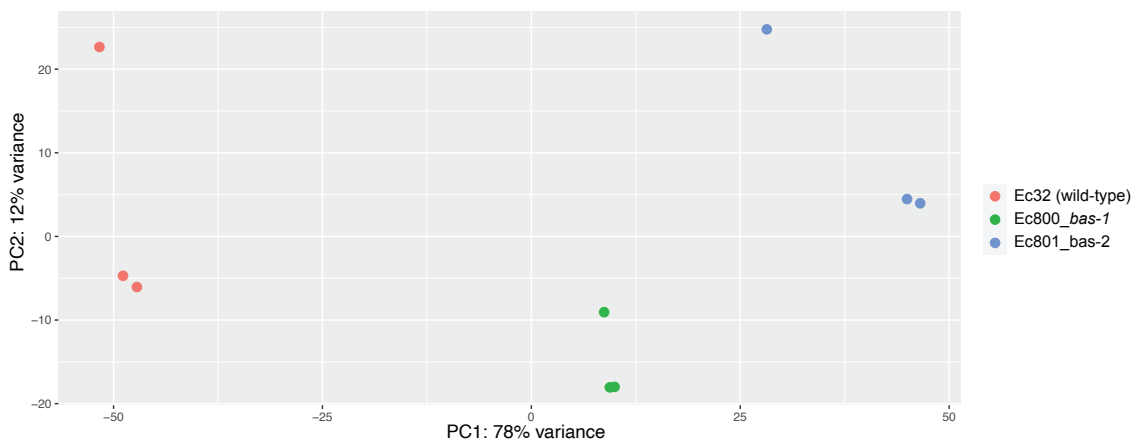
615 **Figure S3.** Morphological phenotypes of diploid sporophytes derived by crossing *dis-2* x *bas-1*  
616 or *dis-1* x *bas-2*. Note that the diploid sporophyte derived from the cross has a wild-type  
617 phenotype, indicating the two mutations complement each other. Scale=20  $\mu\text{m}$ .



618

619

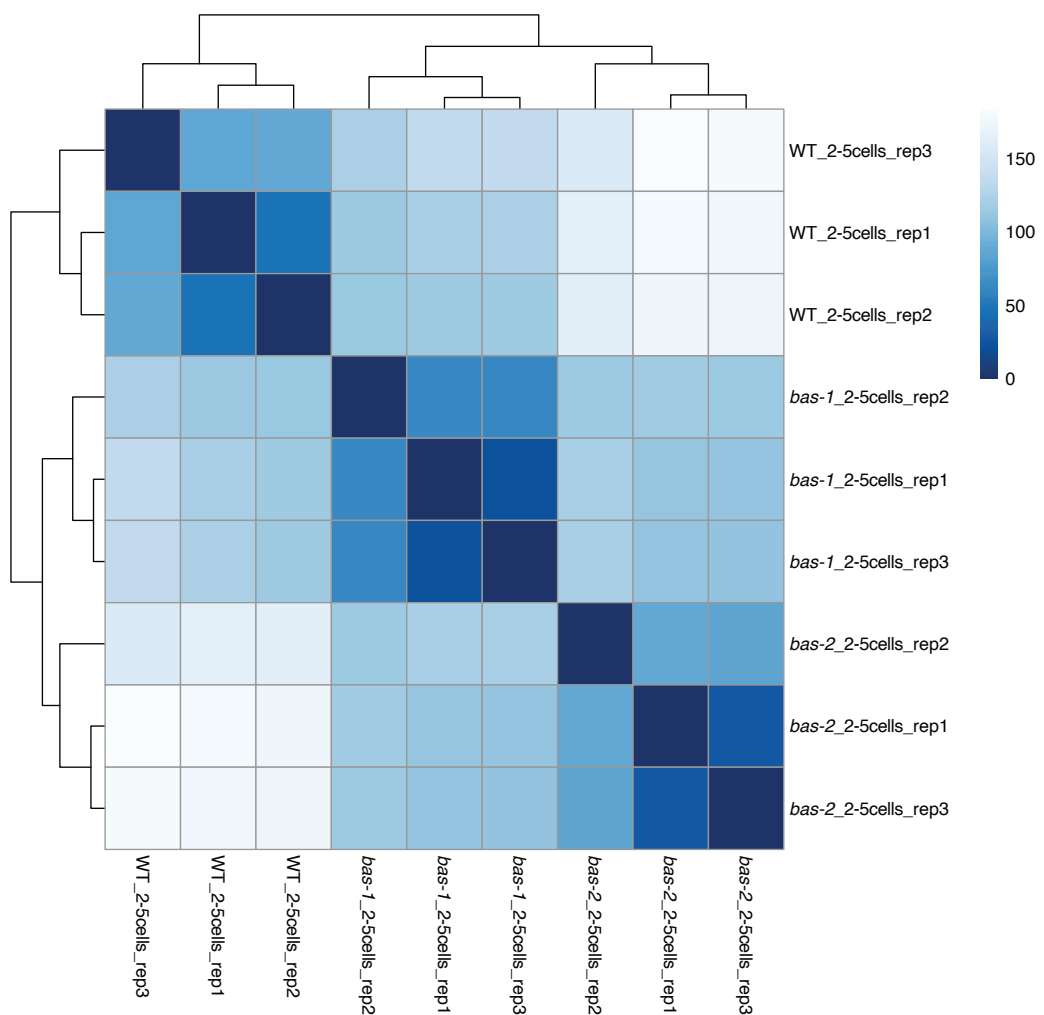
620 **Figure S4.** Principal component analysis (PCA) comparison of transcript abundance patterns for  
621 all expressed genes across wild-type (WT), *bas-1* and *bas-2* replicate samples. The two  
622 dimensions represent 78% and 12% of the variance. The analysis was carried out using  
623 normalized counts generated by DESeq2 after Variance Stabilizing Transformation (VST).



624

625

626 **Figure S5.** Between-sample correlation diagnostics of the RNA sequencing data. Heat map  
627 representing the distance between replicates. Euclidian distances were calculating from  
628 normalized counts generated by DESeq2 after Variance Stabilizing Transformation (VST). Details  
629 of the samples are given in Table S7.

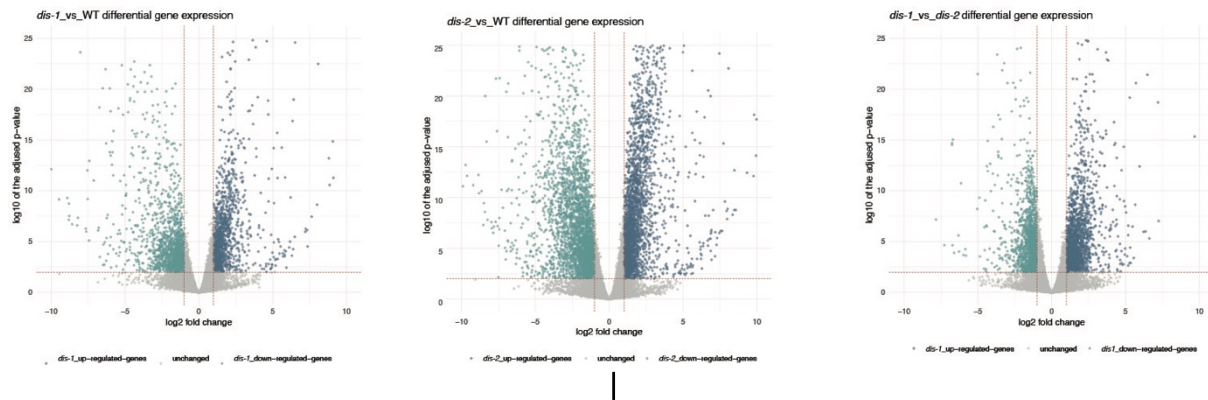


630

631

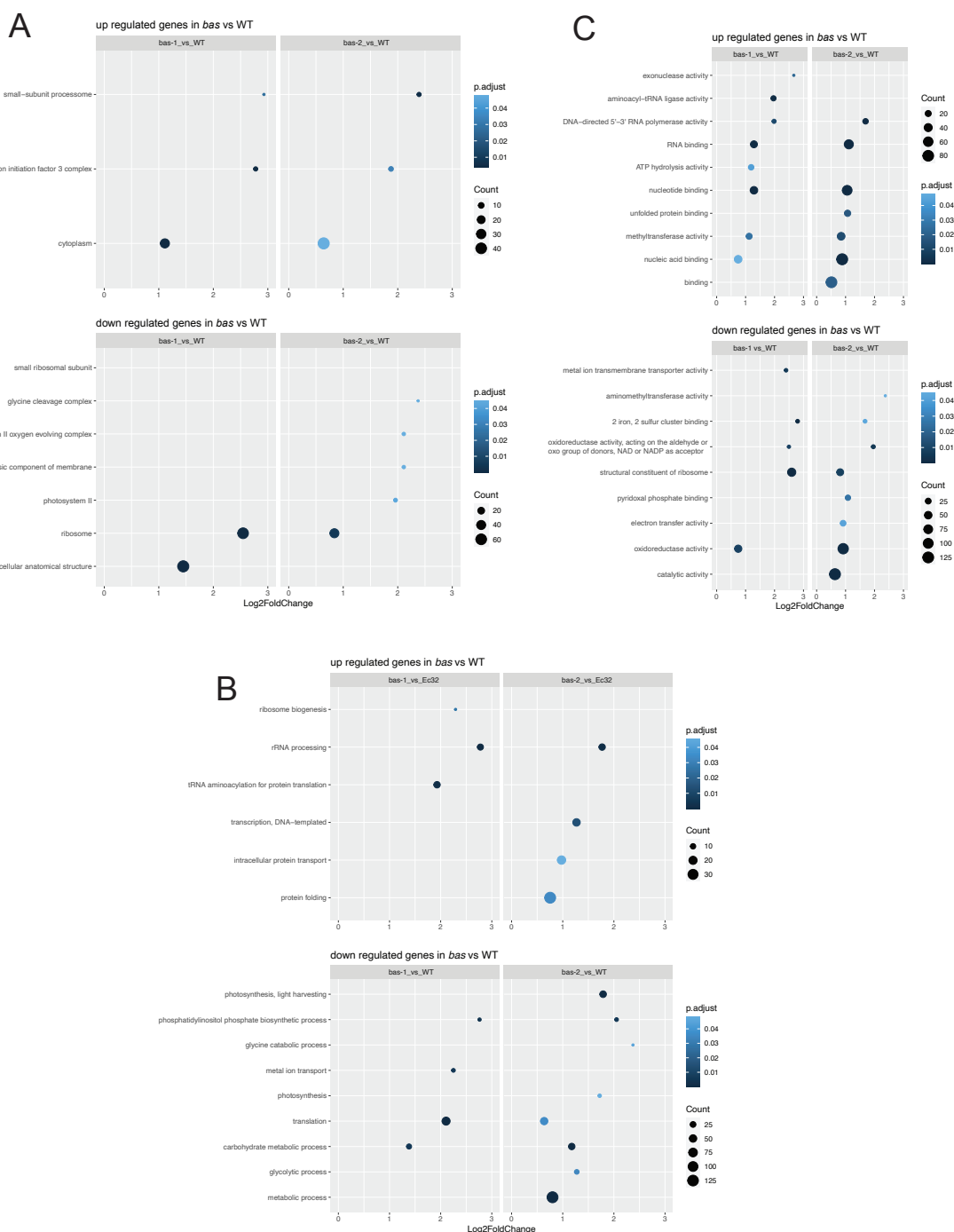
632

633 **Figure S6.** Vulcano plots of all genes in pairwise comparisons between wild-type (WT) and  
634 mutants (*bas-1* and *bas-2*). The log2 FC value was calculated based on the mean expression  
635 level (TPM) for each gene. Each dot represents one gene. Blue represents upregulated genes  
636 and green downregulated genes in each comparison.



637  
638

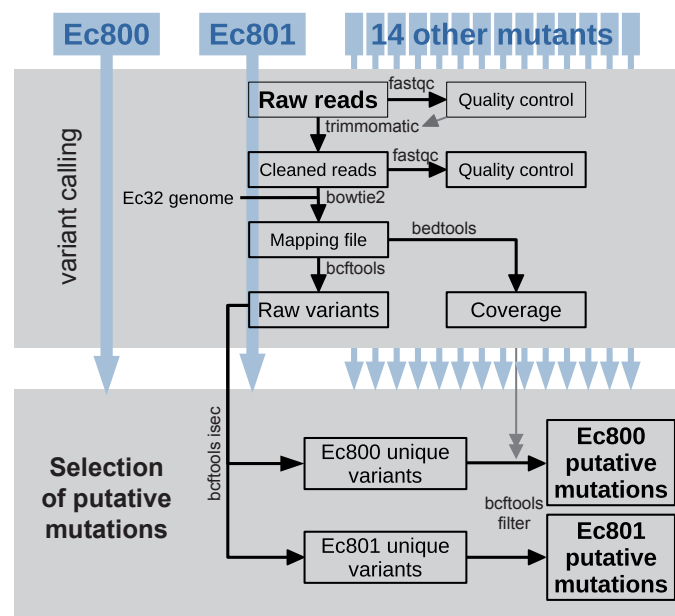
639 **Figure S7.** GO term enrichment observed in DE gene sets in bas mutants compared to WT. Dot  
 640 plot representation is divided according to GO term ontology classes 'Cellular Component' (A),  
 641 'Molecular Function' (B) and 'Biological Processes' (C).



642  
 643

644 **Figure S8.** Schematic diagram of the approach used to detect putative mutations in the  
645 genomes of Ec800 and Ec801.

646



647

648

## 649 References

650 André, J., Harrison, S., Towers, K., Qi, X., Vaughan, S., McKean, P. G. and Ginger, M. L. (2013).  
651 The tubulin cofactor C family member TBCCD1 orchestrates cytoskeletal filament  
652 formation. *J. Cell Sci.* **126**, 5350–5356.

653 Arun, A., Coelho, S. M., Peters, A. F., Bourdareau, S., Peres, L., Scornet, D., Strittmatter, M.,  
654 Lipinska, A. P., Yao, H., Godfroy, O., et al. (2019). Convergent recruitment of TALE  
655 homeodomain life cycle regulators to direct sporophyte development in land plants and  
656 brown algae. *eLife* **8**,

657 Atkinson, J. A., Rasmussen, A., Traini, R., Voß, U., Sturrock, C., Mooney, S. J., Wells, D. M. and  
658 Bennett, M. J. (2014). Branching out in roots: uncovering form, function, and regulation.  
659 *Plant Physiol.* **166**, 538–550.

660 Avia, K., Coelho, S. M., Montecinos, G. J., Cormier, A., Lerck, F., Mauger, S., Faugeron, S., Valero,  
661 M., Cock, J. M. and Boudry, P. (2017). High-density genetic map and identification of  
662 QTLs for responses to temperature and salinity stresses in the model brown alga  
663 *Ectocarpus*. *Sci. Rep.* **7**, 43241.

664 Badis, Y., Scornet, D., Harada, M., Caillard, C., Godfroy, O., Raphalen, M., Gachon, C. M. M.,  
665 Coelho, S. M., Motomura, T., Nagasato, C., et al. (2021). Targeted CRISPR-Cas9-based  
666 gene knockouts in the model brown alga *Ectocarpus*. *New Phytol.* **231**, 2077–2091.

667 Bayer, M., Slane, D. and Jürgens, G. (2017). Early plant embryogenesis-dark ages or dark matter?  
668 *Curr. Opin. Plant Biol.* **35**, 30–36.

669 Berger, F., Taylor, A. and Brownlee, C. (1994). Cell fate determination by the cell wall in early  
670 fucus development. *Science* **263**, 1421–1423.

671 Bisgrove, S. R. and Kropf, D. L. (1998). Alignment of centrosomal and growth axes is a late event  
672 during polarization of *Pelvetia compressa* zygotes. *Dev. Biol.* **194**, 246–256.

673 Bogaert, K. A., Arun, A., Coelho, S. M. and De Clerck, O. (2013). Brown algae as a model for plant  
674 organogenesis. *Methods Mol. Biol. Clifton NJ* **959**, 97–125.

675 Bogaert, K. A., Zakka, E. E., Coelho, S. M. and De Clerck, O. (2022). Polarization of brown algal  
676 zygotes. *Semin. Cell Dev. Biol.* S1084-9521(22)00075–1.

677 Bolger, A. M., Lohse, M. and Usadel, B. (2014). Trimmomatic: a flexible trimmer for Illumina  
678 sequence data. *Bioinforma. Oxf. Engl.* **30**, 2114–2120.

679 Bothwell, J. H., Marie, D., Peters, A. F., Cock, J. M. and Coelho, S. M. (2010). Cell cycles and  
680 endocycles in the model brown seaweed, *Ectocarpus siliculosus*. *Plant Signal. Behav.* **5**,  
681 1473–1475.

682 Bouget, F. Y., Gerttula, S., Shaw, S. L. and Quatrano, R. S. (1996). Localization of Actin mRNA  
683 during the Establishment of Cell Polarity and Early Cell Divisions in *Fucus* Embryos. *Plant*  
684 *Cell* **8**, 189–201.

685 **Bourdareau, S.** (2018). Contrôle génétique et épigénétique des transitions du cycle de vie chez  
686 l'algue brune *Ectocarpus* sp.

687 **Bourdareau, S., Tirichine, L., Lombard, B., Loew, D., Scornet, D., Wu, Y., Coelho, S. M. and Cock,**

688 J. M. (2021). Histone modifications during the life cycle of the brown alga *Ectocarpus*.  
689 *Genome Biol.* **22**, 12.

690 **Brownlee, C. and Bouget, F. Y.** (1998). Polarity determination in *Fucus*: from zygote to  
691 multicellular embryo. *Semin. Cell Dev. Biol.* **9**, 179–185.

692 **Cock, J. M., Godfroy, O., Macaisne, N., Peters, A. F. and Coelho, S. M.** (2014). Evolution and  
693 regulation of complex life cycles: a brown algal perspective. *Curr. Opin. Plant Biol.* **17**, 1–  
694 6.

695 **Cock, J. M., Liu, F., Duan, D., Bourdareau, S., Lipinska, A. P., Coelho, S. M. and Tarver, J. E.** (2017).  
696 Rapid Evolution of microRNA Loci in the Brown Algae. *Genome Biol. Evol.* **9**, 740–749.

697 **Coelho, S. M., Peters, A. F., Charrier, B., Roze, D., Destombe, C., Valero, M. and Cock, J. M.** (2007).  
698 Complex life cycles of multicellular eukaryotes: New approaches based on the use of  
699 model organisms. *Gene* **406**, 152–170.

700 **Coelho, S. M., Godfroy, O., Arun, A., Le Corguillé, G., Peters, A. F. and Cock, J. M.** (2011).  
701 OUROBOROS is a master regulator of the gametophyte to sporophyte life cycle transition  
702 in the brown alga *Ectocarpus*. *Proc. Natl. Acad. Sci. U. S. A.* **108**, 11518–11523.

703 **Coelho, S. M., Scornet, D., Rousvoal, S., Peters, N., Darteville, L., Peters, A. F. and Cock, J. M.**  
704 (2012a). Genetic crosses between *Ectocarpus* strains. *Cold Spring Harb. Protoc.* **2012**,  
705 262–265.

706 **Coelho, S. M., Scornet, D., Rousvoal, S., Peters, N. T., Darteville, L., Peters, A. F. and Cock, J. M.**  
707 (2012b). How to cultivate *Ectocarpus*. *Cold Spring Harb. Protoc.* **2012**, 258–261.

708 **Coelho, S. M., Scornet, D., Rousvoal, S., Peters, N., Darteville, L., Peters, A. F. and Cock, J. M.**  
709 (2012c). Immunostaining of *Ectocarpus* cells. *Cold Spring Harb. Protoc.* **2012**, 369–372.

710 **Coelho, S. M., Peters, A. F., Müller, D. and Cock, J. M.** (2020). *Ectocarpus*: an evo-devo model for  
711 the brown algae. *EvoDevo* **11**, 19.

712 **Cormier, A., Avia, K., Sterck, L., Derrien, T., Wucher, V., Andres, G., Monsoor, M., Godfroy, O.,**

713 Lipinska, A., Perrineau, M.-M., et al.

714 (2017). Re-annotation, improved large-scale  
715 assembly and establishment of a catalogue of noncoding loci for the genome of the  
model brown alga *Ectocarpus*. *New Phytol.* **214**, 219–232.

716 **Cossard, G. G., Godfroy, O., Nehr, Z., Cruaud, C., Cock, J. M., Lipinska, A. P. and Coelho, S. M.**  
717 (2022). Selection drives convergent gene expression changes during transitions to co-  
718 sexuality in haploid sexual systems. *Nat. Ecol. Evol.* **6**, 579–589.

719 **Creyghton, M. P., Roël, G., Eichhorn, P. J. A., Hijmans, E. M., Maurer, I., Destréé, O. and Bernards,**

720 R.

721 (2005). PR72, a novel regulator of Wnt signaling required for Naked cuticle function.  
*Genes Dev.* **19**, 376–386.

722 **Feldman, J. L. and Marshall, W. F.** (2009). ASQ2 encodes a TBCC-like protein required for mother-  
723 daughter centriole linkage and mitotic spindle orientation. *Curr. Biol. CB* **19**, 1238–1243.

724 **Godfroy, O., Peters, A. F., Coelho, S. M. and Cock, J. M.** (2015). Genome-wide comparison of  
725 ultraviolet and ethyl methanesulphonate mutagenesis methods for the brown alga  
726 *Ectocarpus*. *Mar. Genomics*.

727 **Godfroy, O., Uji, T., Nagasato, C., Lipinska, A. P., Scornet, D., Peters, A. F., Avia, K., Colin, S., Laure,**  
728 **M., Motomura, T., et al.** (2017). DISTAG/TBCCd1 Is Required for Basal Cell Fate  
729 Determination in *Ectocarpus*. *Plant Cell*.

730 **Goncalves, J., Nolasco, S., Nascimento, R., Lopez Fanarraga, M., Zabala, J. C. and Soares, H.**  
731 (2010). TBCCD1, a new centrosomal protein, is required for centrosome and Golgi  
732 apparatus positioning. *EMBO Rep.* **11**, 194–200.

733 **Goodner, B. and Quatrano, R. S.** (1993). Fucus Embryogenesis: A Model to Study the  
734 Establishment of Polarity. *Plant Cell* **5**, 1471–1481.

735 **Gschloessl, B., Guermeur, Y. and Cock, J. M.** (2008). HECTAR: a method to predict subcellular  
736 targeting in heterokonts. *BMC Bioinformatics* **9**, 393.

737 **Hutlin, E. L., Ting, L., Bruckner, R. J., Gebreab, F., Gygi, M. P., Szpyt, J., Tam, S., Zarraga, G., Colby,**  
738 **G., Baltier, K., et al.** (2015). The BioPlex Network: A Systematic Exploration of the Human  
739 Interactome. *Cell* **162**, 425–440.

740 **Hutlin, E. L., Bruckner, R. J., Paulo, J. A., Cannon, J. R., Ting, L., Baltier, K., Colby, G., Gebreab, F.,**  
741 **Gygi, M. P., Parzen, H., et al.** (2017). Architecture of the human interactome defines  
742 protein communities and disease networks. *Nature* **545**, 505–509.

743 **Kimata, Y., Higaki, T., Kawashima, T., Kurihara, D., Sato, Y., Yamada, T., Hasezawa, S., Berger, F.,**  
744 **Higashiyama, T. and Ueda, M.** (2016). Cytoskeleton dynamics control the first  
745 asymmetric cell division in *Arabidopsis* zygote. *Proc. Natl. Acad. Sci. U. S. A.* **113**, 14157–  
746 14162.

747 **Kumar, S., Stecher, G. and Tamura, K.** (2016). MEGA7: Molecular Evolutionary Genetics Analysis  
748 Version 7.0 for Bigger Datasets. *Mol. Biol. Evol.* **33**, 1870–1874.

749 **Langmead, B. and Salzberg, S. L.** (2012). Fast gapped-read alignment with Bowtie 2. *Nat. Methods* **9**, 357–359.

751 **Lipinska, Cormier, A., Luthringer, R., Peters, A. F., Corre, E., Gachon, C. M. M., Cock, J. M. and**  
752 **Coelho, S. M.** (2015). Sexual dimorphism and the evolution of sex-biased gene  
753 expression in the brown alga *Ectocarpus*. *Mol. Biol. Evol.* **32**, 1581–1597.

754 **Lipinska, A. P., Serrano-Serrano, M. L., Cormier, A., Peters, A. F., Kogame, K., Cock, J. M. and**  
755 **Coelho, S. M.** (2019). Rapid turnover of life-cycle-related genes in the brown algae. *Genome Biol.* **20**, 35.

757 **Love, M. I., Huber, W. and Anders, S.** (2014). Moderated estimation of fold change and  
758 dispersion for RNA-seq data with DESeq2. *Genome Biol.* **15**, 550.

759 760 **Lowe, D. G.** (2004). Distinctive Image Features from Scale-Invariant Keypoints. *International Journal of Computer Vision* **60**, 91–110.

761 762 763 764 **Macaisne, N., Liu, F., Scornet, D., Peters, A. F., Lipinska, A., Perrineau, M.-M., Henry, A., Strittmatter, M., Coelho, S. M. and Cock, J. M.** (2017). The Ectocarpus IMMEDIATE UPRIGHT gene encodes a member of a novel family of cysteine-rich proteins that have an unusual distribution across the eukaryotes. *Dev. Camb. Engl.*

765 766 **Mongera, A., Michaut, A., Guillot, C., Xiong, F. and Pourquié, O.** (2019). Mechanics of Anteroposterior Axis Formation in Vertebrates. *Annu. Rev. Cell Dev. Biol.* **35**, 259–283.

767 768 769 **Montecinos, A., Valero, M., Guillemin, M.-L., Peters, A., Desrut, A. and Couceiro, L.** (2017). Species delimitation and phylogeographic analyses in the Ectocarpus subgroup siliculosi (Ectocarpales, Phaeophyceae). *J. Phycol.* **53**, 17–31.

770 771 772 **Nithianantham, S., Le, S., Seto, E., Jia, W., Leary, J., Corbett, K. D., Moore, J. K. and Al-Bassam, J.** (2015). Tubulin cofactors and Arl2 are cage-like chaperones that regulate the soluble  $\alpha\beta$ -tubulin pool for microtubule dynamics. *eLife* **4**, e08811.

773 774 775 776 **Peters, A. F., Scornet, D., Ratin, M., Charrier, B., Monnier, A., Merrien, Y., Corre, E., Coelho, S. M. and Cock, J. M.** (2008). Life-cycle-generation-specific developmental processes are modified in the immediate upright mutant of the brown alga Ectocarpus siliculosus. *Development* **135**, 1503–1512.

777 778 **Radoeva, T., Vaddepalli, P., Zhang, Z. and Weijers, D.** (2019). Evolution, Initiation, and Diversity in Early Plant Embryogenesis. *Dev. Cell* **50**, 533–543.

779 780 **Read, C., Walther, P. and von Einem, J.** (2021). Quantitative Electron Microscopy to Study HCMV Morphogenesis. *Methods Mol. Biol. Clifton NJ* **2244**, 265–289.

781 782 **Ren, H., Rao, J., Tang, M., Li, Y., Dang, X. and Lin, D.** (2022). PP2A interacts with KATANIN to promote microtubule organization and conical cell morphogenesis. *J. Integr. Plant Biol.*

783 784 **Reynhout, S. and Janssens, V.** (2019). Physiologic functions of PP2A: Lessons from genetically modified mice. *Biochim. Biophys. Acta Mol. Cell Res.* **1866**, 31–50.

785 786 787 **Rose, L. and Gönczy, P.** (2014). Polarity establishment, asymmetric division and segregation of fate determinants in early *C. elegans* embryos. *WormBook Online Rev. C Elegans Biol.* 1–43.

788 789 790 **Shaw, S. L. and Quatrano, R. S.** (1996). The role of targeted secretion in the establishment of cell polarity and the orientation of the division plane in *Fucus* zygotes. *Dev. Camb. Engl.* **122**, 2623–2630.

791 792 793 **Spinner, L., Pastuglia, M., Belcram, K., Pegoraro, M., Goussot, M., Bouchez, D. and Schaefer, D. G.** (2010). The function of TONNEAU1 in moss reveals ancient mechanisms of division plane specification and cell elongation in land plants. *Dev. Camb. Engl.* **137**, 2733–2742.

794 795 **Stamatakis, A.** (2014). RAxML version 8: a tool for phylogenetic analysis and post-analysis of large phylogenies. *Bioinforma. Oxf. Engl.* **30**, 1312–1313.

796 **Takahashi, M., Shibata, H., Shimakawa, M., Miyamoto, M., Mukai, H. and Ono, Y. (1999).**  
797 Characterization of a novel giant scaffolding protein, CG-NAP, that anchors multiple  
798 signaling enzymes to centrosome and the golgi apparatus. *J. Biol. Chem.* **274**, 17267–  
799 17274.

800 **Tang, D., Mar, K., Warren, G. and Wang, Y. (2008).** Molecular mechanism of mitotic Golgi  
801 disassembly and reassembly revealed by a defined reconstitution assay. *J. Biol. Chem.*  
802 **283**, 6085–6094.

803 **Tian, G., Huang, Y., Rommelaere, H., Vandekerckhove, J., Ampe, C. and Cowan, N. J. (1996).**  
804 Pathway leading to correctly folded beta-tubulin. *Cell* **86**, 287–296.

805 **Tsugama, D., Yoon, H. S., Fujino, K., Liu, S. and Takano, T. (2019).** Protein phosphatase 2A  
806 regulates the nuclear accumulation of the *Arabidopsis* bZIP protein VIP1 under hypo-  
807 osmotic stress. *J. Exp. Bot.* **70**, 6101–6112.

808 **Ueda, M. and Berger, F. (2019).** New cues for body axis formation in plant embryos. *Curr. Opin.*  
809 *Plant Biol.* **47**, 16–21.

810 **Umen, J. and Coelho, S. (2019).** Algal sex determination and the evolution of anisogamy. *Annu.*  
811 *Rev. Microbiol.* **73**, 267–291.

812 **Van Leene, J., Blomme, J., Kulkarni, S. R., Cannoot, B., De Winne, N., Eeckhout, D., Persiau, G.,**  
813 **Van De Slijke, E., Vercruyse, L., Vanden Bossche, R., et al. (2016).** Functional  
814 characterization of the *Arabidopsis* transcription factor bZIP29 reveals its role in leaf and  
815 root development. *J. Exp. Bot.* **67**, 5825–5840.

816 **Wlodarchak, N. and Xing, Y. (2016).** PP2A as a master regulator of the cell cycle. *Crit. Rev.*  
817 *Biochem. Mol. Biol.* **51**, 162–184.

818 **Wurzenberger, C. and Gerlich, D. W. (2011).** Phosphatases: providing safe passage through  
819 mitotic exit. *Nat. Rev. Mol. Cell Biol.* **12**, 469–482.

820 **Xu, H., Ginsburg, K. S., Hall, D. D., Zimmermann, M., Stein, I. S., Zhang, M., Tandan, S., Hill, J. A.,**  
821 **Horne, M. C., Bers, D., et al. (2010).** Targeting of protein phosphatases PP2A and PP2B  
822 to the C-terminus of the L-type calcium channel Ca v1.2. *Biochemistry* **49**, 10298–10307.

823 **Yadav, L., Tamene, F., Göös, H., van Drogen, A., Katainen, R., Aebersold, R., Gstaiger, M. and**  
824 **Varjosalo, M. (2017).** Systematic Analysis of Human Protein Phosphatase Interactions  
825 and Dynamics. *Cell Syst.* **4**, 430-444.e5.

826 **Yu, G., Wang, L.-G., Han, Y. and He, Q.-Y. (2012).** clusterProfiler: an R package for comparing  
827 biological themes among gene clusters. *Omics J. Integr. Biol.* **16**, 284–287.

828 **Zwaenepoel, K., Goris, J., Erneux, C., Parker, P. J. and Janssens, V. (2010).** Protein phosphatase  
829 2A PR130/B'alpha1 subunit binds to the SH2 domain-containing inositol polyphosphate  
830 5-phosphatase 2 and prevents epidermal growth factor (EGF)-induced EGF receptor  
831 degradation sustaining EGF-mediated signaling. *FASEB J. Off. Publ. Fed. Am. Soc. Exp.*  
832 *Biol.* **24**, 538–547.

